Eur. Phys. J. E **2**, 377–402 (2000)

THE EUROPEAN PHYSICAL JOURNAL E

EDP Sciences

Elastic rod model of a supercoiled DNA molecule

C. Bouchiat[1,a] and M. Mézard[1,2]

[1] Laboratoire de Physique Théorique de l'Ecole Normale Supérieure,[b] 24 rue Lhomond 75231 Paris Cedex 05, France
[2] Institute for Theoretical Physics, University of California Santa Barbara, CA 93106-4030, USA

Received 1 April 1999 and Received in final form 4 January 2000

Abstract. We study the elastic behaviour of a supercoiled DNA molecule. The simplest model is that of a rod-like chain, involving two elastic constants, the bending and the twist rigidities. Writing this model in terms of Euler angles, we show that the corresponding Hamiltonian is singular and needs a small distance cut-off, which is a natural length scale giving the limit of validity of the model, of the order of the double-helix pitch. The rod-like chain in the presence of the cut-off is able to reproduce quantitatively the experimentally observed effects of supercoiling on the elongation-force characteristics, in the small supercoiling regime. An exact solution of the model, using both transfer matrix techniques and its mapping to a quantum mechanics problem, allows to extract, from the experimental data, the value of the twist rigidity. We also analyse the variation of the torque and the writhe-to-twist ratio *versus* supercoiling, showing analytically the existence of a rather sharp crossover regime which can be related to the excitation of plectoneme-like structures. Finally we study the extension fluctuations of a stretched and supercoiled DNA molecule, both at fixed torque and at fixed supercoiling angle, and we compare the theoretical predictions to some preliminary experimental data.

PACS. 87.15.By Structure and bonding – 61.41.+e Polymers, elastomers, and plastics

1 Introduction

During the last few years, single molecule biophysics has become a very active field of research. Among the new explored areas, one finds the study of elastic properties of biopolymers, in particular the DNA molecule, under physical conditions close to that encountered in living organisms [1–3]. The theoretical work reported in the present paper was motivated by the results of micromanipulation experiments being performed at Ecole Normale Supérieure [3] with an isolated DNA molecule, immersed in a solution of given salinity at room temperature. One extremity of the molecule is biochemically bound at multiple sites to a treated glass cover slip. The other end is similarly attached to a paramagnetic bead with a radius of a few microns which is performing a Brownian motion in the solution. An appropriate magnetic device is able to pull and rotate at the same time the magnetic bead. Because of the multiple attachments of the molecule extremities, the rotation of the bead results in a supercoiling constraint for the DNA isolated molecule.

When no rotation is applied on the bead, the force *versus* extension curves are very well described [4] by a simple elastic model, the so-called Worm-Like Chain (WLC) model which describes a phantom chain using a single elastic constant, the bending rigidity [5]. This model reproduces the data within experimental accuracy, in a very wide range of pulling force from $F \simeq 0.01\,\mathrm{pN}$ to $F \simeq 10\,\mathrm{pN}$. One has to go up to 70 pN to leave the elastic regime and see a sharp increase of the molecule length which is associated with a transition to a new molecular phase, the "S-DNA" [6].

In contrast, in stretching experiments performed with supercoiled DNA molecules [3,7], two molecular structural transitions appear within a more restricted domain of forces. An instructive way to display the supercoiled DNA stretching data is to plot the molecule extension *versus* the degree of supercoiling σ (defined as the ratio of the number of bead turns to the number of double-helix turns in the relaxed molecule), at various fixed values of the stretching force. Three such plots are shown in Figure 1 for typical force values. Working with molecules having a moderate degree of supercoiling, $\sigma \leq 0.1$, two changes of regime occur in the force range between $F = 0.01\,\mathrm{pN}$ and $F = 5.0\,\mathrm{pN}$. For forces below 0.44 pN the extension *versus* supercoiling curves are symmetric under the exchange $\sigma \to -\sigma$ and have been called "hat" curves for obvious reasons. This is the domain of entropic elasticity which will be our main topic in the present paper. When $F \geq 0.5\,\mathrm{pN}$ a plateau is developed in the underwinding region $\sigma < 0$. The mechanical underwinding energy is transformed into chemical energy which is used to open up the hydrogen bonds and denaturation bubbles appear along the DNA

[a] e-mail: `claude.bouchiat@lpt.ens.fr`
[b] UMR 8549: Unité Mixte du Centre National de la Recherche Scientifique et de l'Ecole Normale Supérieure.

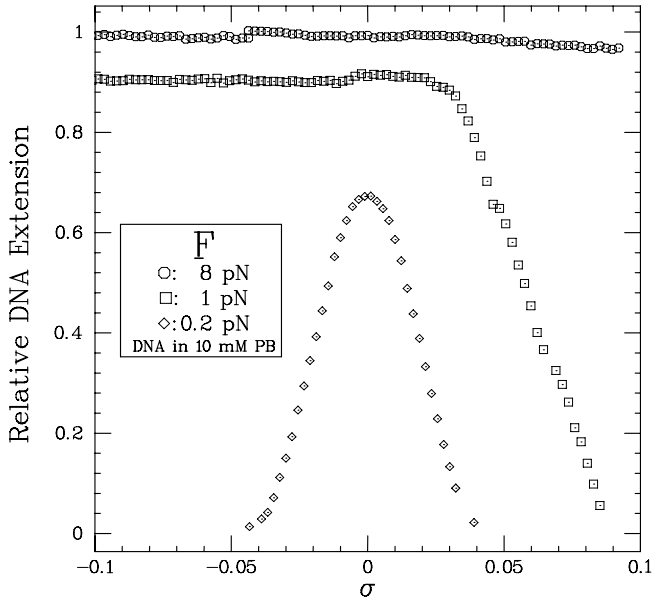

Fig. 1. The elongation *versus* the reduced supercoiling parameter $\sigma = n/L_{k0}$, where L_{k0} stands for the number of double-helix turns in the absence of external constraints. The curve $F = 0.2\,\mathrm{pN}$, a typical "hat" curve, corresponds to the regime of entropic elasticity which is well described by the RLC model introduced in the present paper. The curve $F = 1\,\mathrm{pN}$ exhibits a plateau in the underwound region ($\sigma < 0$) which is associated with the denaturation of the DNA. In the third curve $F = 8\,\mathrm{pN}$, a second plateau has developed for ($\sigma > 0$); it has been interpreted as an induced transition to a new structure of DNA: the "P-DNA".

chain. Above 4 pN, a plateau appears also in the overwinding region $\sigma > 0$. This has been interpreted as a transition to a new structure of DNA called the "P-DNA" [11]. The double-helix structure is clearly responsible for the ability of DNA to convert mechanical torsional energy into chemical energy, with a net preference for underwinding energy.

Our work here will be restricted to the entropic elastic regime, and its aim is primarily to compute the extension *versus* supercoiling hat curves. We have used the simplest extension of the WLC model, which is still a phantom chain, with one single new elastic constant, the twist rigidity. We call the corresponding model a Rod-Like Chain (RLC). We will show that the RLC model, described in terms of local Euler angle variables, is singular in the limit of a purely continuous chain. Its physical realization requires the introduction of a short length scale cut-off (which will turn out to be of the order of magnitude of the double-helix pitch). Then the RLC is able to reproduce all experimental data in the restricted domain of its validity which we have discussed above. The good fit to the experimental data allows to deduce the twist rigidity to bending rigidity ratio, which was rather poorly known so far (with uncertainties up to a factor or 2). A short account of some parts of this work has been discussed in a previous letter [12] (where the RLC model appeared under a slightly different name: the WLRC model). We shall give here a more comprehensive—and hopefully comprehensible—description of our model. Our principal aim is to show how the RLC model, once it has been properly formulated, can be solved exactly: by exact, we mean that the predictions of the model can be computed by a mixture of analytic and numerical methods to any desired precision.

The first conclusive work able to fit the experimental data from a rod-like chain with two elastic constants is that of Marko and Vologodskii [30], who used a discretized model and performed some Monte Carlo simulations. On the analytical side, Fain *et al.* [25] wrote the elastic energy in terms of a local writhe formula, similarly to the one which we have used, but they used it only in the zero temperature limit [16]. In an independent work which appeared just after ours, Moroz and Nelson [21] used the same form of energy as we did, but with a different approach for handling the singularity of the model in the continuum limit. We shall comment extensively on the differences of these approaches, as well as on the obtained results.

Developing a theory beyond the elastic regime is a much more difficult task, since such a theory should involve both the self-repulsion of the chain (necessary to prevent a collapse of plectonemes), and the possibility of denaturation. Some first attempts in these directions can be found in [13,14]. Recently an explicit model, coupling the hydrogen-bond opening with the untwisting of the double helix, has been proposed [15]. It leads to a unified description of thermal and untwisting DNA denaturation in the high stretching force limit.

We now indicate the organization of the paper, with some emphasis upon the "RLC model crisis" and its solution. In section 2 we introduce the RLC model and discuss its range of validity. We note first that the elastic energy used in the present paper is invariant under rotation about the molecular axis, in apparent contradiction with the double-helix structure. We prove that added cylindrical asymmetric terms in the elastic energy are washed out by averaging upon the empirical length resolution Δl, about three times the double-helix pitch p. We also discuss the relationship to the quantum mechanics problem of a symmetric top, which appears naturally when one considers the configurations of the DNA chain as world lines in a quantum-mechanical problem. We stress that, despite a formal analogy, there is an important difference in the formulation of the two problems. The RLC analog of the angular momentum is not quantized since, in contrast to the symmetric top, the physical states of an elastic rod are not invariant under rotations of 2π about its axis. This is the origin of the "RLC crisis".

In section 3 we incorporate in the RLC partition function the supercoiling constraint coming from the rotation of the magnetic bead. First written as a boundary condition upon Euler angles used to specify the DNA configuration, the supercoiling constraint is transformed, assuming some regularity conditions on the Euler angles, into an equality between the bead rotation angle and the sum of the twist and writhe variables of the open molecular chain.

These variables fluctuate independently in the absence of supercoiling so that the constrained RLC partition function is given as a convolution product of the twist and writhe partition functions. The writhe partition function Fourier transform is in correspondence with the quantum mechanics problem of a charged particle moving in the field of a magnetic monopole with an unquantized charge. The spontaneous fluctuations of the writhe provide a spectacular signature of the RLC model pathology: the second moment of the fluctuation is predicted to be infinite in the continuum limit. This divergence comes from a singularity appearing in the RLC potential when the molecular axis is antiparallel to the stretching force.

Section 4 explains how the angular cut-off needed in order to transform the RLC model into a sensible one can be generated by the discretization of the chain. The introduction of a length cut-off b, of the order Δl, appears rather natural since a length average upon Δl has been invoked to justify our choice of the RLC elastic energy. We proceed next with the development of the two main tools used to get an exact solution of the discretized RLC model: a direct transfer matrix approach and a quantum mechanics approach involving a regularized RLC Hamiltonian with a potential derived from the discretized model and now free from any singularity.

In section 5 we use the two above methods in order to compute the elongation *versus* supercoiling characteristics of a long DNA chain. The results are compared with experimental data in section 7 where the small distance cut-off b and the twist elastic constant are determined.

Section 6 presents a complementary approach, that of Monte Carlo simulations which provides the only method so far to introduce the constraints of self-avoidance and knots elimination. After a presentation of the results of Marko and Vologodskii [30], we describe our less ambitious simulations which were used to validate our analytic method.

In section 8 we use the RLC model to analyse, at a force taken on the high side of our explored area, the variation of the torque and the writhe-to-twist ratio *versus* supercoiling. The two curves exhibit a rather sharp change of regime near one given value of the supercoiling angle: the torque, after a nearly linear increase, becomes almost supercoiling independent while the writhe-to-twist ratio, initially confined to the 20% level, develops a fast linear increase. We give arguments suggesting that this quasi-transition is associated with the creation of plectoneme-like configurations, able to absorb supercoiling at constant torque.

Finally section 9 studies, within the RLC model, the extension fluctuations of an isolated DNA molecule, subject both to stretching and supercoiling constraints. The predictions are made for two thermodynamic ensembles: one at fixed torque, the other at fixed supercoiling angle. Although the two ensembles lead, as they should, to identical results as far as average values are concerned, they yield widely different predictions for the extension fluctuations above a certain supercoiling threshold (close to the one appearing in the previous section): the fixed torque ensemble becomes much more noisy. We give a qualitative explanation for this peculiar behaviour and compare our predictions to some preliminary experimental data at fixed supercoiling.

In section 10 we give a summary of the work and some perspectives on its future extensions.

2 Elastic energy of the rod-like chain

A given configuration of the rod-like chain (RLC) is specified, in the continuous limit, by the local orthonormal trihedron $\{\hat{\mathbf{e}}_i(s)\} = \{\hat{\mathbf{u}}(s), \hat{\mathbf{n}}(s), \hat{\mathbf{t}}(s)\}$, where s is the arc length along the molecule, $\hat{\mathbf{t}}$ is the unit vector tangent to the chain, $\hat{\mathbf{u}}(s)$ is along the basis line and $\hat{\mathbf{n}}(s) = \hat{\mathbf{t}}(s) \wedge \hat{\mathbf{u}}(s)$. The evolution of the trihedron $\{\hat{\mathbf{e}}_i(s)\}$ along the chain is obtained by applying a rotation $\mathcal{R}(s)$ to a reference trihedron $\{\hat{\mathbf{e}}_i^0(s)\}$ attached to a rectilinear relaxed molecule: $\hat{\mathbf{e}}_i(s) = \mathcal{R}(s) \cdot \hat{\mathbf{e}}_i^0(s)$.

The rotation $\mathcal{R}(s)$ is parameterized by the usual three Euler angles $\theta(s)$, $\phi(s)$ and $\psi(s)$. The reference trihedron is such that $\theta(s) = 0$, $\phi(s) + \psi(s) = \omega_0 s$, where ω_0 is the rotation per unit length of the base axis in the relaxed rectilinear DNA molecule. With the above definition, the set of s-dependent Euler angles $\theta(s)$, $\phi(s), \psi(s)$ describes the general deformations of the DNA molecule with respect to the relaxed rectilinear configuration. It is now convenient to introduce the angular velocity vector $\boldsymbol{\Omega}(s)$ associated with the rotation $\mathcal{R}(s)$. The evolution of the trihedron $\{\hat{\mathbf{e}}_i(s)\}$ along the molecular chain is given in term of $\boldsymbol{\Omega}(s)$ by the set of equations:

$$\frac{\mathrm{d}}{\mathrm{d}s}\,\hat{\mathbf{e}}_i(s) = \big(\boldsymbol{\Omega}(s) + \omega_0 \hat{\mathbf{t}}(s)\big) \wedge \hat{\mathbf{e}}_i(s). \tag{1}$$

We shall use in the following the components of $\boldsymbol{\Omega}(s)$ along the trihedron $\{\hat{\mathbf{e}}_i(s)\}$: $\Omega_i = \boldsymbol{\Omega}(s) \cdot \hat{\mathbf{e}}_i(s)$, with $\hat{\mathbf{e}}_1 = \hat{\mathbf{u}}$, $\hat{\mathbf{e}}_2 = \hat{\mathbf{n}}$ and $\hat{\mathbf{e}}_3 = \hat{\mathbf{t}}$. (The Ω_i are computed in terms of the Euler angles and their s derivatives in the Appendix A.) The stretched RLC energy E_{RLC} is written as a line integral along the chain of length L, involving a sum of three contributions:

$$E_{\mathrm{RLC}} = k_{\mathrm{B}}T \int_0^L \mathrm{d}s \big(\mathcal{E}_{\mathrm{bend}}(s) + \mathcal{E}_{\mathrm{twist}}(s) + \mathcal{E}_{\mathrm{stretch}} f(s)\big). \tag{2}$$

The above bend, twist and stretch linear energy densities are given by

$$\begin{aligned}
\mathcal{E}_{\mathrm{bend}} &= \frac{A}{2}\big(\Omega_1^2 + \Omega_2^2\big) = \frac{A}{2}\left|\frac{\mathrm{d}\hat{\mathbf{t}}(s)}{\mathrm{d}s}\right|^2 = \frac{A}{2}\big(\dot{\phi}^2 \sin^2\theta + \dot{\theta}^2\big), \\
\mathcal{E}_{\mathrm{twist}} &= \frac{C}{2}\Omega_3^2 = \frac{C}{2}(\dot{\psi} + \dot{\phi}\cos\theta)^2, \\
\mathcal{E}_{\mathrm{stretch}} &= -\hat{\mathbf{t}}(s) \cdot \mathbf{F}/(k_{\mathrm{B}}T) = -\frac{F\cos\theta}{k_{\mathrm{B}}T},
\end{aligned} \tag{3}$$

where the dot stands for the s derivative.

$\mathcal{E}_{\mathrm{bend}}$ is proportional to the inverse of the square of the curvature radius and represents the resistance against

bending around an axis perpendicular to the chain axis. The coefficient A is the persistence length; its typical value is 50 nm.

$\mathcal{E}_{\rm twist}$ is proportional to the square of the projection of the angular velocity along the molecular axis and gives the energy associated with a twist constraint. The twist rigidity C is known to be in the range 50 to 100 nm; its determination from the experimental measurement will be the topic of section 7.

$\mathcal{E}_{\rm strech}$ is the potential energy associated with the uniform stretching force $\mathbf{F} = F \cdot \hat{\mathbf{z}}$, which is applied at the free end of the molecule; it is written as a line integral involving $\hat{\mathbf{t}}(s) \cdot \hat{\mathbf{z}}$.

The ground-state configurations of the rod-like chain have been studied in [16]. These may apply to the properties of small plasmids, but in the regime which we are interested in, the thermal fluctuation effects are crucial. If no twist-dependent properties are imposed or measured, one can factor out the ψ integral in the partition function, or equivalently use the $C = 0$ theory, in which case one recovers the elastic energy of the Worm-Like Chain model:

$$\frac{E_{\rm WLC}}{k_{\rm B}T} = \int_0^L {\rm d}s \left(\frac{A}{2} \left| \frac{{\rm d}\hat{\mathbf{t}}(s)}{{\rm d}s} \right|^2 - \cos\theta(s) F/(k_{\rm B}T) \right). \quad (4)$$

It is now appropriate to raise two questions about the above formulas.

2.1 Is a cylindrical symmetric elastic rigidity tensor adequate for the DNA chain?

The theory which we are using here is an elastic theory which cannot be valid down to atomic scales. In particular it does not take into account the microscopic charges on the DNA and their Coulomb interactions in the solvent, but it just describes the net effect by a set of elastic constants. However, even at the level of an elastic description, one may wonder whether our choice of elastic tensor, which ignores the helical structure of the DNA, is valid. Indeed the elastic energy given by equations (3) involves a rigidity tensor with a cylindrical symmetry around the molecular axis $\hat{\mathbf{t}}(s)$. We would like to argue that such a description is a reasonable approximation if one deals with experimental data obtained with a finite length resolution $\Delta l \simeq 10$ nm, as is the case for the experiments we shall analyse. The pitch p of the double helix contains approximately 10 basis which corresponds to a length of 3.4 nm. A simple way to break the cylindrical symmetry is to introduce in the elastic energy linear density a term proportional to $\Delta\Omega(s) = \Omega_1^2 - \Omega_2^2$. As is shown in Appendix A, $\Delta\Omega(s)$ can be written in terms of the Euler angles in the following way:

$$\Delta\Omega(s) = {\Omega_\perp}^2 \cos 2\left(\zeta(s) + \psi(s) + \frac{2\pi s}{p} \right),$$

with ${\Omega_\perp}^2 = \Omega_1^2 + \Omega_2^2$ and $\zeta(s) = \arctan(\dot{\theta}/(\sin\theta\dot{\phi}))$.

One must note that $\Delta\Omega(s)$ oscillates with a wavelength which is half the pitch p of the double helix. An average involving a resolution length, about 6 times the oscillation wavelength, is expected to lead to a strong suppression of $\Delta\Omega(s)$. The average $\overline{\Delta\Omega(s)} = \int {\rm d}s_1 P(s_1 - s)\Delta\Omega(s_1)$, associated with the resolution function $P(s) = (1/\sqrt{2\pi}\Delta l)\exp(-\frac{1}{2}s^2/\Delta l^2)$, is computed explicitly in Appendix A in terms of simple Gauss integrals, assuming that the phase $\zeta(s) + \psi(s)$ and the amplitude ${\Omega_\perp}^2$ vary linearly within the interval $(s - \Delta l, s + \Delta l)$. Ignoring first the $\Omega_\perp$ variation and assuming that the supercoiling angle per unit length is $\ll \omega_0$, we arrive in Appendix A at the result:

$$\overline{\Delta\Omega(s)} \approx \Delta\Omega(s) \exp\left(-\frac{1}{2}\left(\frac{4\pi\Delta l}{p} \right)^2 \right).$$

Taking $p = 3.4$ nm, $\Delta l = 10$ nm, one gets $(4\pi\Delta l/p) \approx 37$; it is clear that the above expression of $\overline{\Delta\Omega(s)}/\Delta\Omega(s)$ is zero for all practical purposes. The extra term $\propto (\partial{\Omega_\perp}^2/\partial s)$ is also found to be exceedingly small. The same suppression factor holds for $\overline{\Omega_1\Omega_2}$, while in the case of $\overline{\Omega_1\Omega_3}$ the argument of the exponential is divided by 4 but with the value quoted above for Δl the suppression effect is still very important. Therefore all the cylindrical asymmetric terms in the elastic rigidity tensor are washed out by the empirical finite length resolution averaging.

In the same spirit there are various effects which are not taken into account by our description. An obvious one is the heterogeneity of the sequence: a more microscopic description should include some fluctuations of the rigidities along the chain, depending on the sequence of bases. However, one expects that such fluctuations will be averaged out on some long length scales, such as those involved in the experimental situation under study. This has been confirmed by some more detailed study involving some simple model of disordered sequences [18]. One should also notice that we have not allowed the total length of the chain to vary. It is possible to add some elastic energy to bond stretching as well as some stretch-twist coupling in order to try to describe the behaviour at rather large forces and supercoiling [19–21]. But as we will see such terms are irrelevant for the elastic regime which we study here.

2.2 What is the precise connection of the elastic rod thermal fluctuations problem with the quantum theory of a symmetric top?

A careful inspection of the formulas (2) and (3) suggests a close analogy of the elastic linear energy density with the classical Lagrangian of the symmetric top, with A and C being, up to a constant factor, the moments of inertia. For given values of the Euler angles $\theta(s)$, $\phi(s)$, $\psi(s)$ at the two ends $s_0 = 0$ and $s_1 = L$ of the chain, the partition function of the RLC model is given by the following path integral:

$$Z(\theta_1, \phi_1, \psi_1, s_1 | \theta_0, \phi_0, \psi_0, s_0) = \int \mathcal{D}(\theta, \phi, \psi) \exp\left(-\frac{E_{\rm RLC}}{k_{\rm B}T} \right), \quad (5)$$

where $\mathcal{D}(\theta,\phi,\psi)$ stands for the integration functional measure for the set of paths joining two points of the Euler angles space with $0 \leq \theta \leq \pi$ but no constraints imposed upon ϕ and ψ. Let us perform in the elastic energy integral over s (Eq. (2)) an analytic continuation towards the imaginary s-axis. We shall use for convenience a system of units where $\hbar = c = k_{\mathrm{B}}T = 1$ and write $\Im s = t$. The elastic energy E_{RLC} is transformed into $-i\int_{t_0}^{t_1} \mathrm{d}t\mathcal{L}(t)$, where the Lagrangian is that of a symmetric top in a static electric field f: $\mathcal{L}(t) = \frac{1}{2}\sum_1^3 C_i\Omega_i^2 + f\cos\theta(t)$, with inertia moments $C_1 = C_2 = A$, $C_3 = C$ and $f = F/(k_{\mathrm{B}}T)$. The analytically continued partition function of the RLC model is then identified with the Feynmann amplitude:

$$\begin{aligned}&\big\langle\theta_1,\phi_1,\psi_1,t_1|\theta_0,\phi_0,\psi_0,t_0\big\rangle = \\ &\int \mathcal{D}(\theta,\phi,\psi)\exp\left(i\int_{t_0}^{t_1}\mathrm{d}t\mathcal{L}(t)\right) = \\ &\Big\langle\theta_1,\phi_1,\psi_1\Big|\exp\Big(-i(t_1-t_0)\hat{\mathcal{H}}_{\mathrm{top}}\Big)\Big|\theta_0,\phi_0,\psi_0\Big\rangle,\end{aligned}$$

where $\hat{\mathcal{H}}_{\mathrm{top}}$ is the symmetric top Hamiltonian written as a second-order differential operator acting upon Euler angles wave functions. Returning to real value of s, one gets the RLC model partition function as a quantum mechanics matrix element, with the substitution $i(t_1-t_0) \to s_1 - s_0$. It is now convenient to introduce the complete set of energy eigenstates of $\hat{\mathcal{H}}_{\mathrm{top}}$: $\hat{\mathcal{H}}_{\mathrm{top}}|n\rangle = E_n|n\rangle$. One gets then

$$\begin{aligned}&Z(\theta_1,\phi_1,\psi_1,s_1|\theta_0,\phi_0,\psi_0,s_0) = \\ &\quad\sum_n \exp(-LE_n)\Psi_n(\theta_1,\phi_1,\psi_1)\Psi_n^\star(\theta_0,\phi_0,\psi_0), \qquad (6)\end{aligned}$$

where $\Psi_n(\theta,\phi,\psi) = \langle\theta,\phi,\psi|n\rangle$ is the eigenfunction relative to the state $|n\rangle$. As we shall discuss later, the interest of the above formula lies in the fact that the above sum is dominated by the term of lowest energy.

At this point one may get the impression that the solution of the RLC model is reduced to a relatively straightforward problem of quantum mechanics. Although this identification is valid in the case of the worm-like chain model (WLC) which describes the entropic elasticity of a stretched DNA molecule with no twist constraints, it is not the case for the more general RLC model. The above analysis was somewhat formal in the sense that the Hamiltonian $\hat{\mathcal{H}}_{\mathrm{top}}$ was given as a differential operator and it is thus not completely defined, until the functional space on which it is acting is properly specified. Physical considerations will lead us to choose different functional spaces for the two problems in hands:

In the symmetric top problem the space is that of 2π periodic functions of the Euler angles ϕ and ψ, but in the study of RLC thermal fluctuations the space is that of general functions of these angles, without any constraint of periodicity.

As an illustration, let us discuss the simple case of a non-flexible rod with $E = \frac{C}{2}k_{\mathrm{B}}T\int_0^L \mathrm{d}s\,\dot{\psi}(s)^2$. The associated quantum problem is the cylindrical rotator described by the Hamiltonian $\hat{\mathcal{H}}_{\mathrm{rot}} = -(1/2C)(\partial^2/\partial\psi^2)$. The 2π periodicity of the motion implies a discrete spectrum for the conjugate momentum $p_\psi = -i(\partial/\partial\psi)$; the corresponding wave function is $\exp(ik\psi)$, where k is an arbitrary integer. Imposing on the molecular chain the boundary conditions $\psi(s_0 = 0) = 0$, $\psi(s_1 = L) = \chi$, the partition function of the non-flexible rod is obtained by a straightforward application of formula (6)

$$Z(\chi,L) = \sum_k \exp\left(ik\chi - \frac{L}{2C}k^2\right).$$

In the experiments to be discussed in the present paper $L \gg C$ and, as a consequence, the sum over the integer k is dominated by the terms $k = 0, \pm 1$, leading to the rather unphysical result: $Z(\chi,L) = 1 + 2\cos\chi\exp(-\frac{L}{2C})$.

On the contrary, in order to describe the twisting of an elastic rod, the spectrum of p_ψ has to be taken as continuous and the discrete sum $\sum_k \cdots$ must be replaced by the integral $\int_{-\infty}^{\infty}\mathrm{d}k/(2\pi)\cdots$, which yields the correct result for the partition function

$$Z(\chi,L) \propto \exp -\left(\frac{C}{2L}\chi^2\right). \qquad (7)$$

Two significant physical quantities can be easily obtained from the above partition function: First, the second moment $\langle\chi^2\rangle$ relative to a situation where χ is no longer constrained but allowed to fluctuate freely. Keeping in mind that $P(\chi) \propto Z(\chi,L)$, one gets $\langle\chi^2\rangle = \frac{L}{C}$. Second, the torque Γ given by the logarithmic derivative of $Z(\chi,L)$ with respect to χ: $\Gamma = k_{\mathrm{B}}T(C\chi/L)$. The above quantities look very reasonable from a physical point of view: $\langle\chi^2\rangle$ scales linearly in L, as expected from the fluctuations of a linear chain with a finite correlation length C and the expression of Γ reproduces an elasticity textbook formula, if one remembers that $k_{\mathrm{B}}TC$ is the usual twist rigidity.

The above considerations may look somewhat simpleminded. It turns out, however, that they have important physical consequences. In order to solve the RLC model, we shall have to deal with a quantum spherical top when its angular momentum along the top axis is not quantized. Such a problem is mathematically singular and, as a consequence, the continuous limit of the RLC model we have considered so far will not give an adequate description of supercoiled DNA. We shall have to introduce a discretized version of the RLC model, involving an elementary length scale b about twice the double-helix pitch p. This is consistent with the considerations of the previous section where the empirical length resolution $\Delta l \approx 3p$ was invoked in order to justify the cylindrical symmetry of the tensor of elastic rigidities.

3 The partition function for supercoiled DNA in the rod-like chain model

3.1 Implementing the experimental supercoiling constraint on the partition function

The first step is to incorporate in the functional integral the supercoiling constraint which results from a rotation

around the stretching force $\mathbf{F}$ of a magnetic bead biochemically glued to the free end of the DNA chain. The rotation $\mathcal{R}$ in terms of the Euler angles is usually written as a product of three elementary rotations, a rotation θ about the y-axis sandwiched between two rotations ψ and ϕ about the z-axis, performed in that order: $\mathcal{R} = R(\hat{\mathbf{z}}, \phi)R(\hat{\mathbf{y}}, \theta)R(\hat{\mathbf{z}}, \psi)$, where $R(\hat{\mathbf{m}}, \gamma)$ stands for a rotation γ about the unit vector $\hat{\mathbf{m}}$. It is convenient, in the present context, to introduce a different form of $\mathcal{R}$ involving a product of two rotations written in terms of a new set of variables, θ, ψ and $\chi = \phi + \psi$: $\mathcal{R} = R(\hat{\mathbf{z}}, \chi)R(\hat{\mathbf{w}}(\psi), \theta)$ where the unit vector $\hat{\mathbf{w}}(\psi)$ lies in the xy plane and is given by $\hat{\mathbf{w}}(\psi) = R(\hat{\mathbf{z}}, -\psi)\hat{\mathbf{y}}$. (See Appendix A for a proof of the identity of the two above forms of $\mathcal{R}$.) Let us consider, before any application of an external rotation, the DNA segment sticking out from the bead. Assume that it is short enough so that its direction is not affected by thermal fluctuations. Its orientation is specified by three Euler angles, $\theta_{\rm in}$, $\psi_{\rm in}$, $\chi_{\rm in}$. If the rotation of the magnetic bead by n turns is performed adiabatically, the final orientation of the molecular end trihedron $\{\hat{\mathbf{e}}_i(L)\}$ is specified by the rotation:

$$\mathcal{R}(L) = R(\hat{\mathbf{z}}, 2\pi n + \chi_{\rm in})R(\hat{\mathbf{w}}(\psi_{\rm in}), \theta_{\rm in}).$$

We can read off easily from the above formula: $\chi(L) = \phi(L)+\psi(L) = 2\pi n+\chi_{\rm in}$. It is reasonable to assume that in the gluing process no large surpercoiling is involved so that the angles $\chi_{\rm in}$ and $\psi_{\rm in}$ do not exceed 2π. As we will see, the relevant scaling variable for the partition function is

$$\eta = \frac{\chi(L)A}{L}. \tag{8}$$

In the experiments to be analyzed in the present paper, $A/L \simeq \frac{1}{300}$ with η of the order of unity, so that $\chi_{\rm in}$ can be safely ignored in comparison to $2\pi n$. In the following we shall drop the L dependence in $\chi(L)$ and write $\chi = 2\pi n = \phi(L) + \psi(L)$. The above equation does not imply that χ is a discrete variable: it is just for practical reasons that the experimentalists perform measurements with an integer number of turns. On the other hand, if we were dealing with a closed DNA chains instead of an open one, the supercoiling angle $\chi(L)$, which is here an arbitrary real, would get replaced by $2\pi L_k$, where the integer L_k is the topological linking number.

3.1.1 A local writhe formula

We make now an assumption which may look, at first sight, somewhat trivial but has, as we shall see, far-reaching consequences:

The Euler angles $\phi(s)$ and $\psi(s)$ are regular enough functions of s to allow the replacement of χ by a line integral involving the sum of Euler angles derivatives, taken along the trajectory Γ of the tip of the tangent vector $\hat{\mathbf{t}}(s)$.

$$\chi = 2\pi n = \phi(L) + \psi(L) = \int_0^L \mathrm{d}s\big(\dot{\psi} + \dot{\phi}\big). \tag{9}$$

It is then convenient to introduce the total twist along the chain T_w which appears as a Gaussian variable in the partition function.

$$T_w = \int_0^L \mathrm{d}s\Omega_3 = \int_0^L \mathrm{d}s\big(\dot{\psi} + \dot{\phi}\cos\theta\big), \tag{10}$$

where $\Omega_3(s)$ is the projection of the instantaneous rotation vector $\boldsymbol{\Omega}$ onto the unit tangent vector $\hat{\mathbf{t}}(s)$, given in terms of Euler angles in Appendix A. We now *define* a "local writhe" contribution χ_W by substracting the total twist T_w from the supercoiling angle χ

$$\chi_W = \chi - T_w = \int_0^L \mathrm{d}s\dot{\phi}(1 - \cos\theta). \tag{11}$$

The above decomposition follows from our analysis of the empirical supercoiling angle and a mere line integral manipulation. This is reminiscent of the decomposition of the linking number into twist and writhe for closed chains [23, 26].

Formula (11) has been first obtained by Fain *et al.* [25] by adapting to the case of open strings a formula first derived by Fuller [24] for closed strings. We have decided to include an explicit derivation here in order to be able to describe some subtleties in its use, which will require some regularization procedure. Since $\hat{\mathbf{t}}(s)$ is a unitary vector, the curve Γ lies upon the sphere S_2 and it is parametrized by the spherical coordinates $(\theta(s), \phi(s))$. This representation is well known to be singular at the two poles $\theta = 0$, $\theta = \pi$ (the choice of the z-axis is not arbitrary but dictated by the experimental conditions: it coincides with the rotation axis of the magnetic bead and gives also the stretching force direction). With the usual convention, θ is required to lie within the interval $[0, \pi]$. This condition plays an essential role in the quantum-like treatment of the WLC and RLC continuous models, to be discussed later on. When the trajectory Γ passes through the poles the restriction imposed upon θ implies that the function $\phi(s)$ suffers form a discontinuity of $\pm\pi$ and this invalidates our derivation of formula (11). To get around this difficulty, we have to pierce the sphere S_2 at the two poles. The two holes are defined by two horizontal circles with an arbitrary small but finite radius ϵ with their centers lying on the z-axis. Note that S_2 has now the topology of a cylinder so that the piercing of the sphere S_2 provides the necessary topological discrimination between the two distinct physical states $(\theta(s), \phi(s), \psi(s))$ and $(\theta(s), \phi(s) + 2\pi n, \psi(s))$. A careful evaluation of formula (11), involving continuously deformed Γ trajectories drawn on the pierced sphere S_2 in order to avoid the poles, gives results in agreement with those given by the non-local closed-loop writhe formula [23], while a naive application of (11) would lead astray.

3.1.2 Solenoid and plectoneme supercoil configurations

To illustrate this point, we shall evaluate χ_W for right-handed solenoid and plectoneme supercoil configurations, having arbitrary orientations. Let us begin with the simple

case where the solenoid superhelix is winding around the z-axis. The tangent vector tip trajectory $\Gamma_{\rm sol}$ consists of n turns along the horizontal circle cut upon the unit sphere S_2 by the horizontal plane $z = \cos\theta_0$ ($\tan\theta_0 = \frac{2\pi R}{P}$, where R and P are, respectively, the radius and the pitch of the superhelix.) The writhe supercoiling angle $\chi_W(\Gamma_{\rm sol})$ is easily seen to be given by $2\pi n(1-\cos\theta_0)$.

The plectoneme supercoil configuration is composed of two interwound superhelices connected by a handle. The helices have opposite axis but the same helicity. The plectoneme $\hat{\mathbf{t}}$ trajectory $\Gamma_{\rm plec}$ is written as the union of three trajectories: $\Gamma_{\rm plec} = \Gamma^1_{\rm sol} \cup \Gamma_{\rm han} \cup \Gamma^2_{\rm sol}$. $\Gamma^1_{\rm sol}$ is just the right-handed solenoid considered above. $\Gamma_{\rm han}$ is associated with the handle connecting the two superhelices and its contribution to χ_W can be neglected in the large n limit. $\Gamma^2_{\rm sol}$ is the tangent vector trajectory generated by the superhelix winding down the z-axis; it is given by performing upon the $\Gamma^1_{\rm sol}$ the transformation defined by the change of spherical coordinates: $\phi' = -\phi$, $\theta' = \pi - \theta$. One readily gets $\chi_W(\Gamma_{\rm plec})$ by writing $\chi_W(\Gamma_{\rm plec}) = \chi_W(\Gamma^1_{\rm sol}) + \chi_W(\Gamma^2_{\rm sol}) = -4\pi n\cos\theta_0$.

We proceed next to the deformation of $\hat{\mathbf{t}}$ trajectories $\chi_W(\Gamma_{\rm sol})$ and $\Gamma_{\rm plec}$ by applying a rotation about the y-axis of an angle α which is going to vary continuously from 0 to π. We will find that a proper use of formula (11) leads to rotation invariant results in the limit of small but finite angular cut-off. As a first step, let us show that $\chi_W(\Gamma)$ can be written as the circulation along Γ of a magnetic monopole vector potential. This technical detour will also be used in the forthcoming derivation of the RLC model Hamiltonian.

3.1.3 The local writhe χ_W as a magnetic monopole potential vector line integral

Our aim is to prove that the writhe supercoiled angle χ_W can be written as the line integral $\int \mathrm{d}\phi A_\phi = \oint \mathbf{A}_m(\mathbf{r})\,\mathrm{d}\mathbf{r}$, where $A_\phi = (1-\cos\theta)$ will be identified as the ϕ spherical component of the potential vector $\mathbf{A}_m(\mathbf{r})$ of a magnetic monopole of charge unity. Following the well-known Dirac procedure, we write $\mathbf{A}_m(\mathbf{r})$ as the potential vector of a thin solenoid of arbitrary long length, the so called Dirac String $\mathcal{L}$, lying along the negative half z-axis:

$$\mathbf{A}_m(\mathbf{r}) = \int_{\mathcal{L}} \mathrm{d}\mathbf{l} \wedge \nabla_r \frac{1}{|\mathbf{r}-\mathbf{l}|} = \frac{\hat{\mathbf{z}}\wedge\mathbf{r}}{r(r+\hat{\mathbf{z}}\cdot\mathbf{r})}, \tag{12}$$

where $\mathbf{l} = u\hat{\mathbf{z}}$ with $-\infty < u \le 0$. Using the above expression of $\mathbf{A}_m(\mathbf{r})$, one derives the two basic equations which allow the writing of χ_W as the circulation of the magnetic monopole potential vector, valid when $r + \hat{\mathbf{z}}\cdot\mathbf{r} > 0$:

$$\mathbf{A}_m(\mathbf{r})\cdot\mathrm{d}\mathbf{r} = (1-\cos\theta)\mathrm{d}\phi, \tag{13}$$

$$\mathbf{B}_m(\mathbf{r}) = \nabla\wedge\mathbf{A}_m(\mathbf{r}) = \frac{\mathbf{r}}{r^3}, \tag{14}$$

where $\mathbf{B}_m(\mathbf{r})$ is indeed the magnetic field produced by the magnetic charge unit.

Let us now define $S_+(\Gamma)$ (respectively, $S_-(\Gamma)$) as the part of the sphere S_2 bounded by the closed circuit Γ which is run anticlockwise (respectively, clockwise) around the surface normal. (Note that $S_+(\Gamma)\cup S_-(\Gamma) = S_2$.) Let us call Σ_ϵ the part of S_2 defined by the south pole hole and assume that $S_+(\Gamma)\cap\Sigma_\epsilon = \emptyset$ (as a consequence $S_-(\Gamma)\cap\Sigma_\epsilon = \Sigma_\epsilon$). Applying the Stokes theorem to formula (14), we can write

$$\chi_W(\Gamma) = \oint_\Gamma \mathbf{A}_m(\mathbf{r})\cdot\mathrm{d}\mathbf{r} = \int\int_{S_+(\Gamma)} \mathrm{d}\mathbf{S}\cdot\mathbf{B}_m(\mathbf{r}) = \mathcal{A}(S_+(\Gamma)), \tag{15}$$

where $\mathcal{A}(S_+(\Gamma))$ is the area of the spherical cap $S_+(\Gamma)$. The closed circuit Γ is assumed here to be run only once; if it is run n times, as in solenoid and plectoneme configurations, $\mathcal{A}(S_+(\Gamma))$ should then be multiplied by n and the formulas obtained before are immediately recovered. A similar formula, valid mod2π, has been derived previously by Fuller [24], in the case of closed molecular chain.

3.1.4 On the rotation invariance of the writhe supercoiling angle χ_W

We are going now to follow the variation of $\chi_W(\Gamma)$ when the initial tangent vector $\hat{\mathbf{t}}$ trajectory Γ_0 is moved continuously upon the sphere by applying a rotation about the y-axis by an angle α, varying continuously from 0 to π: $\Gamma_0 \Longrightarrow \Gamma(\alpha) = R(\hat{\mathbf{y}},\alpha)\Gamma_0$. We shall choose $\Gamma_0 = \Gamma_{\rm sol}$ but the following analysis can be easily extended to plectonemes or more general configurations involving closed $\hat{\mathbf{t}}$ trajectories.

The crossing of the north pole is harmless because $1-\cos\theta$ vanishes at $\theta = 0$ and everything goes smoothly until $\Gamma(\alpha)$ meets the south pole hole ($\theta = \pi$) when α is approaching $\pi - \theta_0$. When $\alpha < \pi - \theta_0$ the south pole stays outside $S_+(\Gamma(\alpha))$ and $\chi_W(\Gamma)$ is given by n times the spherical cap area: $\mathcal{A}(S_+(\Gamma(\alpha)) = \mathcal{A}(S_+(\Gamma_0)) = 2\pi(1-\cos\theta_0)$. In other words $\chi_W(\Gamma(\alpha)) = \chi_W(\Gamma_0)$ if $\alpha < \pi - \theta_0$.

In order to avoid the hole $\Gamma(\alpha)$ must be continuously deformed for $\alpha > \pi - \theta_0$ into the circuit $\Gamma'(\alpha) = \Gamma(\alpha)\cup\Gamma_\epsilon$, where the path Γ_ϵ consists in n turns run anticlockwise around the south pole hole of radius ϵ. (We ignore the two-way narrow lane connecting the two loops which gives a vanishing contribution.) It is clear now that $S_+(\Gamma(\alpha))$ contains the south pole, so we must apply the Stokes theorem to the clockwise spherical bowl $S_-(\Gamma(\alpha))$:

$$\chi_W(\Gamma(\alpha)) = -n\int\int_{S_-(\Gamma(\alpha))} \mathrm{d}\mathbf{S}\cdot\mathbf{B}_m(\mathbf{r}) = -n\mathcal{A}(S_-(\Gamma(\alpha)) = n(\mathcal{A}(S_+(\Gamma(\alpha)) - 4\pi).$$

The contribution of the path Γ_ϵ is readily found to be $4\pi n(1+O(\epsilon^2))$ so it just cancels the $-4\pi n$ term in the above result. As a consequence, the writhe supercoiling angle associated with the south pole avoiding $\hat{\mathbf{t}}$ trajectory $\chi_W(\Gamma'(\alpha))$ coincides when $\pi - \theta_0 < \alpha < \pi$, with the $\alpha = 0$ initial result: $\chi_W(\Gamma'(\alpha)) = \chi_W(\Gamma_0) = 2\pi n(1-\cos\theta_0)$ up to corrections $O(\epsilon^2)$.

In conclusion, we have shown that a proper use of formula (11)*, in the simple case of solenoidal configurations, leads to rotation invariant χ_W in the limit of small ϵ.*

This result can be easily extended to the plectonemic configurations and even to more general ones. The crucial cancellation is taking place in the vicinity of the south pole crossing and thus does not depend on the detailed shape closed trajectory Γ_0 in the $\hat{\mathbf{t}}$ space. If one adds the minimal extra string section to the solenoid or plectoneme, necessary to get a closed loop in the physical space, our findings are in agreement, in the limit of large n, with those obtained from the non-local closed loop writhe formula [23], which is explicitly rotation invariant from the start. Formula (11) is thus a correct description of the problem provided the trajectory is obtained from the straight line ($\theta(s) = 0$, $\phi(s) = 0$) by a continuous transformation on the unit sphere pierced at $\theta = \pi$. A similar condition was obtained by Fuller [24] in his local Writhe formula for closed strings. An alternative derivation of our result, more similar to the approach of Fain [25], could be to close the open string by some straight line closing at infinity and rely on Fuller's formula, but this procedure raises subtle questions about the contribution of added pieces which made us prefer the present explicit derivation.

3.2 The rod-like chain Hamiltonian

The partition function for a fixed value of χ is given by the path integral in the space of Euler angles

$$Z(\chi, F) = \int \mathcal{D}(\theta, \phi, \psi)\delta\Big(\chi - \int_0^L \mathrm{d}s\big(\dot{\phi} + \dot{\psi}\big)\Big) \times \exp -\frac{E_{\mathrm{RLC}}}{k_{\mathrm{B}}T}. \tag{16}$$

The functional space $\theta(s)$, $\phi(s)$, $\psi(s)$ should be specified in accordance with the previous considerations, in particular the tangent vector $\hat{\mathbf{t}}$ paths must bypass the holes on the pierced sphere S_2. This can be achieved by introducing explicitly in E_{RLC} a short-range repulsive potential near $\theta = \pi$.

Two extra constraints, non-local in the tangent vector $\hat{\mathbf{t}}$ space should have been, in principle, implemented in the above partition function.

The first one concerns self-avoidance effects induced by the screened Coulomb repulsion between different molecular sections. Even the simple version of this constraint, used in supercoiled plasmids Monte Carlo simulations [29], is exceedingly difficult to implement in the quantum mechanics inspired formalism of the present paper. Here Coulomb-induced self-avoidance will be ignored as all quantitative analytic approaches did so far, including the celebrated WLC computation. It will appear that these effects play a limited role in the low supercoiling regime ($|\sigma| \leq 0.02$) to be analyzed in the present paper, a regime and experimental conditions where the WLC model is also working beautifully.

The second non-local constraint not implemented in the present work concerns the exclusion of knotted chain configurations. In principle, knotting an open DNA chain is not forbidden, but such a transition is expected to be inhibited on the time scale of the actual experiment since the contour length of the molecule L is only 1.7 times the circumference of the bead glued at the free end of the molecule.

Using a Fourier representation of the Dirac δ-function, we can write the partition function as a Fourier integral: $Z(\chi, F) = \int \mathrm{d}k \exp(-ik\chi)\tilde{Z}(k)$, where the Fourier transform $\tilde{Z}(k)$ is given by the functional integrals:

$$\tilde{Z}(k) = \int \mathcal{D}(\theta, \phi) \exp\left(ik\chi_W - \frac{\mathcal{E}_{\mathrm{bend}} + \mathcal{E}_{\mathrm{stretch}}}{k_{\mathrm{B}}T}\right)\tilde{Z}_T(k),$$
$$\tilde{Z}_T(k) = \int \mathcal{D}(\psi) \exp\Big(ikT_w - \frac{\mathcal{E}_{\mathrm{twist}}}{k_{\mathrm{B}}T}\Big), \tag{17}$$

where the above factorization follows from the identity $\int_0^L \mathrm{d}s(\dot{\phi}+\dot{\psi}) = T_w + \chi_W$, using the elastic energy densities defined in (3). The Gaussian path integral upon ψ is readily performed and gives the Fourier transform of the twist partition function of equation (7) $\tilde{Z}_T(k) = \exp(-\frac{k^2 L}{2C})$, up to a trivial constant. The partition function Fourier transform $\tilde{Z}(k)$ can then be written as the product $\tilde{Z}(k) = \tilde{Z}_T(k)\tilde{Z}_W(k)$ where $\tilde{Z}_W(k)$, which is interpreted as the writhe partition function Fourier transform, is given by a path integral upon θ and ϕ, with the effective energy

$$\tilde{E}_W(k) = \frac{E_{WLC}}{k_{\mathrm{B}}T} + ik\chi_W. \tag{18}$$

Using the results of the previous section ones sees immediately that $ik\chi_W$ can be written as i times the line integral $\int \mathbf{A}_m(\mathbf{r})\,\mathrm{d}\mathbf{r}$, where $\mathbf{A}_m(\mathbf{r})$ is the vector potential produced by the magnetic monopole, having now a charge k. If one performs, as in section 3.2, an analytic continuation of the integral over s in $\tilde{E}_W(k)$ towards the imaginary axis, the i factor disappears in the writhe line integral. One arrives at the action integral of a unit charge particle moving on the unit sphere under the joint action of an electric field f and a magnetic monopole of charge k. In order to get the corresponding Hamiltonian $\hat{H}_{\mathrm{RLC}}(k)$, we apply a standard quantum mechanics rule used to implement the switching on of a magnetic field: we replace in the kinetic terms $\frac{1}{2A}\mathbf{p}^2$, the particle momentum $\mathbf{p}$ by $\mathbf{p} - e\mathbf{A}_m(\mathbf{r})$ (here e=1). The term linear in $\mathbf{A}_m(\mathbf{r})$ disappears by averaging over the final angle $\phi = \phi(L)$ and we are left with the diamagnetic term

$$\frac{1}{2A}\mathbf{A}_m^2(\mathbf{r}) = \frac{k^2}{2A}\,\frac{1-\cos\theta}{1+\cos\theta}. \tag{19}$$

Adding (19) to the WLC Hamiltonian, one arrives at the dimensionless Hamiltonian $\hat{H}_{\mathrm{RLC}}(k)$ associated with the partition function $\tilde{Z}_W(k)$:

$$\hat{H}_{\mathrm{RLC}}(k) = -\frac{1}{2\sin\theta}\,\frac{\partial}{\partial\theta}\sin\theta\frac{\partial}{\partial\theta} - \alpha\cos\theta + \frac{k^2}{2}\,\frac{1-\cos\theta}{1+\cos\theta}, \tag{20}$$

where we have taken, as the length unit, the persistence length A and introduced the dimensionless force parameter $\alpha = \frac{FA}{k_B T}$.

Let us stress that the above Hamiltonian is a straightforward consequence of the expression for the elastic energy (Eqs. (2), (3)) and our expression (9) giving the supercoiling constraint χ in terms of Euler angles derivatives.

Moreover, as is shown in Appendix B, $\hat{H}_{\rm RLC}(k)$ can be derived directly, *without having to introduce the local writhe given by formula (11).* The method involves the quantization of the symmetric top Hamiltonian as a differential operator acting upon non-periodic functions of the Euler angles ϕ and ψ. This is required to describe the thermal fluctuations of an elastic rod (see section 2.2) and k appears as the continuous angular momentum along the top axis.

Introducing the eigenstates and the eigenvalues of $\hat{H}_{\rm RLC}$, $\hat{H}_{\rm RLC}\,\Psi_n(k,\theta) = \epsilon_n(\alpha,k^2)\Psi_n(k,\theta)$, the Fourier-transformed partition function $\tilde{Z}$ can be written as the sum

$$\tilde{Z} = \sum_n \Psi_n(k,\theta_0)\Psi_n(k,\theta_L) \times \exp\left(-\frac{L}{A}\left(\epsilon_n(\alpha,k^2) + \frac{k^2 A}{2C}\right)\right). \quad (21)$$

(Note that $\hat{H}_{\rm RLC}$ being a real operator, the eigenfunctions can always be taken as real.)

In the large L limit, the sum over the eigenstates is dominated by the one with lowest energy $\epsilon_0(\alpha,k^2)$, if $L/A \gg \Delta\epsilon$, where $\Delta\epsilon$ is the energy gap between the ground state and the nearest excited state of $\hat{H}_{\rm RLC}$. This gives the approximate expression for the partition function $Z(\chi,F)$:

$$Z \simeq \int \mathrm{d}k \, \exp\left(-\frac{L}{A}\left(\epsilon_0(\alpha,k^2) + \frac{k^2 A}{2C}\right) - ik\chi\right). \quad (22)$$

To get the above equation, we have also neglected in $\tilde{Z}(k)$ the prefactor involving the ground-state wave function: $\Psi_0(k,\theta_0)\Psi_0(k,\theta_L)$. It leads to finite-size corrections of order A/L, which are in general dominant with respect to those associated with the excited states, which scale as $\exp(-\Delta\epsilon L/A)$.

3.3 The pathology of the RLC model in the continuous limit

In order to comply with the prescription given for the path integral (16), we should have added to $\hat{H}_{\rm RLC}(k)$ a strong repulsive potential acting in the interval $\pi - \epsilon < \theta < \pi$, in order to avoid the $\theta = \pi$ singular point. We shall refer to the $\epsilon \to 0$ limit as the "continuous limit", and show that in that limit the model is pathological. A similar pathology was known to appear in the continuum limit of the winding distribution of random walks [28].

Let us derive from the ground-state energy $\epsilon_0(\alpha,k^2)$ of the Hamiltonian $\hat{H}_{\rm RLC}$ some observable properties of a long RLC. In the following the variable $z = k^2$ is assumed to take positive real values.

If instead of constraining χ one measures its thermal fluctuations, their probability distribution is just $P(\chi) \propto Z$. Let us consider the second moment as we did in section 2.2 for the case of a non-flexible rod.

$$\langle\chi^2\rangle = -\lim_{k^2\to 0}\frac{1}{\tilde{Z}(k)}\frac{\partial^2\tilde{Z}(k)}{\partial k^2} \quad (23)$$

$$= \frac{L}{C} + \frac{2L}{A}\lim_{k^2\to 0}\frac{\partial\epsilon_0(\alpha,k^2)}{\partial k^2}. \quad (24)$$

We recognize in the first term of equation (24) the contribution to $\langle\chi^2\rangle$ from the twist fluctuations, $\frac{L}{C}$, obtained previously. The second piece of (24) gives the contribution from $\langle\chi_W^2\rangle$, but it turns out to be divergent. Evaluating $\epsilon_0(\alpha,k^2)$ at small k^2 from standard perturbation theory, we find $\langle {\chi_W}^2\rangle = (L/A)\langle\Phi_0|(1-\cos\theta)/(1+\cos\theta)|\Phi_0\rangle$, where $\Phi_0(\theta)$ is the ground-state eigenfunction of the WLC Hamiltonian (which is $\hat{H}_{\rm RLC}$ at $k=0$). As $\Phi_0(\theta=\pi)\neq 0$ (for any finite force), we get clearly a logarithmically divergent result. To study analytically this peculiar theory, two methods have been followed, associated with different limits.

i) *The weak force limit*: When $\alpha = 0$ the eigenvalue problem for $H_{\rm RLC}$ can be solved exactly. The eigenfunctions are given in terms of Jacobi polynomials:

$$\Psi_n(k,\theta) = (1+\cos\theta)^k P_n^{(0,2k)}(\cos\theta)$$

and the associated eigenvalues are

$$\epsilon_0\big(\alpha=0,k^2\big) = \frac{(2n+1)k + n^2 + n}{2}.$$

In the presence of a small force ($\alpha \ll 1$), the ground-state energy shift is easily calculated to second order in α:

$$\delta_2\epsilon_0(\alpha,k^2) = -\frac{\alpha k}{1+k} - \frac{\alpha^2}{(1+k)^3(3+2k)}.$$

Note that $\epsilon_0(\alpha,k^2)$ is not an analytic function of $z = k^2$.

ii) *The small k limit*: In order to build a perturbative expansion near $k = 0$, it is convenient to factorize in the wave function the singular term near $\theta = \pi$ by writing: $\Psi_0(k,\theta) = (1+\cos\theta)^k\chi_0(k,\theta)$. The wave function $\chi_0(k,\theta)$ obeys a new wave equation which is amenable to a well-defined perturbation expansion in k. It will turn out that the values of k relevant for the evaluation of Fourier transform are of the order of A/L, so that a first-order perturbation is sufficient (at least when α is small enough in order to guarantee that $\Phi_0(\pi)^2$ stays of the order of unity). We have found that the ground-state energy is given to first order in k by: $\epsilon_0(\alpha,k^2) = \epsilon_0(\alpha,0) + k\Phi_0(\pi)^2 + O(k^2)$. It can be checked that the perturbation result of method i) is consistent with the above equation. The Fourier integral can be readily performed, leading to a Cauchy-type probability distribution, which is

best expressed in terms of the reduced variable $\eta = \chi A/L$: $P(\eta) \simeq (\frac{1}{\pi})\Phi_0(\pi)^2/(\Phi_0(\pi)^4+\eta^2)$ and thus leading to a diverging second moment. This last point can also be seen from the fact that $(\partial\epsilon_0(\alpha,k^2)/\partial k^2) \propto (1/k)$ in the small k limit. The relative extension of the chain in the direction of the force is given by $\langle z\rangle/L = (A/L)(\partial \ln Z/\partial\alpha)$. The partition function in the present case is easily found to be $Z(\eta,\alpha) \propto \exp(-L/A\epsilon_0(\alpha,0))P(\eta)$. It leads to $\langle z\rangle/L = -\frac{\partial\epsilon_0}{\partial\alpha}(\alpha,0) + O(A/L)$, *i.e.* the same result as the WLC model.

The present computations show that the continuous RLC model leads to predictions which are both pathogical (infinite second moment of the writhe spontaneous fluctuations) and in striking contradiction with experiment (absence of variation of the average extension with respect to the supercoiling angle χ at moderate forces). All these peculiar features have been confirmed with explicit computations using a regularized $H_{\rm RLC}$ Hamiltonian. We have indeed found that $\langle\chi_W^2\rangle$ scales like $(L/A)\log(1/\epsilon)$ and that the extension versus supercoiling curves flatten up in the small ϵ limit.

As a last remark we would like to note that if the variable z is continued analytically towards negative value $z \to -\kappa^2$ the ground-state energy develops an imaginary part. This is a clear indication that $\hat{H}_{\rm RLC}(i\kappa)$ has no stable ground state.

4 Discretization as a regularization method for the rod-like chain model

The introduction by hand of an angular cut-off near $\theta = \pi$ appears as an *ad hoc* procedure. We are going to show in the present section that a discretization of the chain involving an elementary link of length b generates an angular cut-off: $\sin^2\theta \geq b/A$. We have seen in section 2.1 that the RLC model with its cylindrical symmetric rigidities tensor is realistic only in the presence of a finite resolution Δl in the length measurement. The existence of a length cut-off $b \sim \Delta l$ appears not only natural but necessary in the present context. The non-trivial fact is that the "mesoscopic" elastic properties, taking place on the length scale of the whole supercoiled molecule (about ten microns) are sensitive to the existence or not of a cut-off in the range of few nanometers. We should also stress that length cut-off effects are found to be reduced to the level of few percents when supercoiling is absent. Therefore in that case the continuous version of the WLC model remains a remarkably good description of the DNA force extension measurements.

Moroz and Nelson [21] have devised a computation procedure where no angular cut-off is introduced from the start. They consider the situation where the torque acting upon the molecular end is kept fixed so that the relevant Hamiltonian is just $\hat{H}_{\rm RLC}(i\kappa)$. The pathology discussed above is expressed in the fact that this Hamiltonian has no stable ground state. In order to deal with such a situation, they use a perturbation method near the high force limit where the relative elongation is close to unity. More precisely, they construct a perturbation expansion involving negative power of $K = \sqrt{\alpha - (1/4)\kappa^2}$. The lowest-order Hamiltonian potential is given, up to a constant, by the small angle approximation $(1/2)K^2\theta^2 = (1/2)(\alpha-(1/4)\kappa^2)\theta^2$. Since $\hat{H}_{\rm RLC}(i\kappa)$ is not a self-adjoint operator, the series diverges and it is expected to be, at best, an asymptotic series. The regime of validity of the prediction is difficult to assess in this approach since one is basically approximating a divergent ground-state energy from the first terms of the perturbation series. As long as one sticks to a finite order, the $\theta = \pi$ singularity does not show up. In order to make contact with experiment, Moroz and Nelson have been forced to restrict their analysis to the domain of force and supercoiling where $K > K_{\rm c} = 3$. In our approach, we have instead regularized the model explicitly, as we shall discuss. This allows to get a better control of the theory and it turns out that our results hold on a much wider range of force-supercoiling. It can even be compared in the $F = 0$ limit to supercoiled plasmids experimental data and Monte Carlo simulations. (See section 8.)

4.1 Construction of the transfer matrix associated with the discretized RLC model

The continuous elastic RLC is transformed into a chain composed of N elementary links of length b. The continuous arc length s is replaced by a discrete set $s_n = nb$, with $0 \leq n \leq N$ and $L = Nb$. We have now to specify the discretization rules. For the bending linear energy density $\mathcal{E}_{\rm bend}$, there is a rather natural prescription: it is to replace $|(\mathrm{d}\hat{\mathbf{t}}(s)/\mathrm{d}s)|^2$ by $(1/b^2)|\hat{\mathbf{t}}_n - \hat{\mathbf{t}}_{n-1}|^2$.

We are led in this way to *the first discretization rule*:

$$\mathcal{E}_{\rm bend} \Longrightarrow \frac{A}{b^2}\big[1-\cos(\theta_n-\theta_{n-1}) + (1-\cos(\phi_n-\phi_{n-1})\sin\theta_n\sin\theta_{n-1})\big]. \quad (25)$$

The above discretized linear density is endowed with a remarkable feature: it is 2π-periodic with respect to the angular finite difference $\phi_n - \phi_{n-1}$. This property plays an essential role in the derivation of the transfer matrix $T(\theta_n,\theta_{n-1})$ which allows a direct computation of the partition function $\tilde{Z}(k)$, averaged upon the azimuthal angle $\phi(L)$.

For the term generated by the supercoiling constraint $ik(1-\cos\theta(s))\dot{\phi}$, we shall impose the same periodicity condition, together with a symmetry under the exchange $\theta_{n+1} \Leftrightarrow \theta_n$, in order to insure the hermiticity of the transfer matrix.

We arrive in this way at *the second discretization rule*:

$$(1-\cos\theta)\dot{\phi} \Longrightarrow \frac{1}{b}\sin\big(\phi_n-\phi_{n-1}\big) \times\left(1-\frac{\cos\theta_n+\cos\theta_{n-1}}{2}\right). \quad (26)$$

The discretized version $\tilde{Z}_N(k,\theta_N,\phi_N)$ of the writhe partition function can be written as the following $2N$ dimension

integral:

$$\tilde{Z}_N\big(k,\theta_N,\phi_N\big)=\int\prod_{n=1}^{N}\mathrm{d}\phi_{n-1}\,d\big(\cos\theta_{n-1}\big)\times\exp-b\big(\Delta\mathcal{E}\big(k,\theta_n,\theta_{n-1},\phi_n-\phi_{n-1}\big)\big),$$

where $\Delta\mathcal{E}(k,\theta_n,\theta_{n-1},\phi_n-\phi_{n-1})$ is the discretized linear energy density obtained from (18) by the replacement rules (25) and (26). It is convenient to introduce the partition function $\tilde{Z}_n(k,\theta_n,\phi_n)$ corresponding to the intermediate value $s_n=bn$. One gets then the recurrence relation

$$\tilde{Z}_n(k,\theta_n,\phi_n)=\int\mathrm{d}\phi_{n-1}\,d(\cos\theta_{n-1})\times\exp-b\left(\Delta\mathcal{E}(k,\theta_n,\theta_{n-1},\phi_n-\phi_{n-1})\right)\times\tilde{Z}_{n-1}(k,\theta_{n-1},\phi_{n-1}).\quad(27)$$

Since we are ultimately interested in the partition function $\tilde{Z}(k)$ averaged upon the azimuthal angle $\phi(L)$, we shall define

$$z_n(k,\theta_n)=\frac{1}{2\pi M}\int_{-\pi M}^{\pi M}\mathrm{d}\phi_n\tilde{Z}_n(k,\theta_n,\phi_n),\quad(28)$$

where M is an integer which can be arbitrarily large. We perform the above integral upon ϕ_n in the two sides of equation (27). In the right-hand side we change the integration variables ϕ_n, ϕ_{n-1} into the new set: $u_n=\phi_n-\phi_{n-1}$, ϕ_{n-1}. Using the periodicity of the integrand with respect to u_n, we can make the replacement

$$\frac{1}{2\pi M}\int_{-\pi M-\phi_{n-1}}^{\pi M-\phi_{n-1}}\mathrm{d}u_n\cdots\Longrightarrow\frac{1}{2\pi}\int_{-\pi}^{\pi}\mathrm{d}u_n\cdots.$$

The integral upon u_n can then be performed exactly in terms of the Bessel function of second type $I_0(z)$ and we arrive finally at an explicit recurrence relation involving the ϕ-average partition function $z_n(k,\theta_n)$:

$$z_n(k,\theta_n)=\int_0^{\pi}\sin\theta_{n-1}\mathrm{d}\theta_{n-1}T(\theta_n,\theta_{n-1})z_{n-1}(k,\theta_{n-1}),\quad(29)$$

$$T(\theta_1,\theta_2,k^2)=\exp-\left\{\frac{A}{b}\big(1-\cos(\theta_1-\theta_2)+\sin\theta_1\sin\theta_2\big)+\frac{b\alpha}{2A}\big(\cos\theta_1+\cos\theta_2\big)\right\}I_0\big(f(\theta_1,\theta_2,k^2)\big),\quad(30)$$

where the Bessel function argument is given by

$$f(\theta_1,\theta_2,k^2)=\sqrt{-k^2\left(1-\frac{\cos\theta_1+\cos\theta_2}{2}\right)^2+\frac{A^2}{b^2}\big(\sin\theta_1\sin\theta_2\big)^2}.\quad(31)$$

To get some basic elements of the transfer matrix formalism, it is useful to rewrite the recursion relation (29) within an operator formalism $|z_n\rangle=\hat{T}(\alpha,k^2)|z_{n-1}\rangle$, where $\hat{T}(\alpha,k^2)$ is the operator associated with the transfer matrix $T(\theta_1,\theta_2,k^2)$. Let us define as $|t_i(\alpha,k^2)\rangle$ the eigenstate of $\hat{T}(\alpha,k^2)$ associated with the eigenvalue $t_i(\alpha,k^2)$. Performing an expansion upon the above set of eigenstates, we can write $|z_N\rangle$ as follows:

$$|z_N\rangle=\hat{T}(\alpha,k^2)^N|z_0\rangle=\sum_i t_i(\alpha,k^2)^N|t_i(\alpha,k^2)\rangle\langle t_i(\alpha,k^2)|z_0\rangle.$$

Let us assume that N is large enough so that the above sum is dominated by the contribution from the lowest eigenvalue. The partition function $Z(\chi)$ can then be written as

$$Z(\chi)=Z\simeq\int\mathrm{d}k\exp\left(-\frac{k^2}{2C}+ik\chi\right)t_0(\alpha,k^2)^N.$$

It is now convenient to introduce the *new definition*

$$\epsilon_0(\alpha,k^2)=-\frac{A}{b}\ln t_0(\alpha,k^2).\quad(32)$$

Note that we had already defined $\epsilon_0(\alpha,k^2)$ as the lowest eigenvalue of H_{RLC}; it is easily verified that the two definitions coincide in the limit $b/A\ll 1$ *modulo* an irrelevant constant. With this new definition equation (22) giving $Z(\chi)$ holds true for the discretized RLC model, within the transfer matrix formalism.

4.2 The angular cut-off induced by the discretization of the RLC model

In this section we are going to discuss what turned out to be a crucial milestone in our work: the understanding that a discretization of the DNA chain could provide the angular cut-off needed to make sense to the RLC model. The first indication came, in fact, from Monte Carlo simulations which will be discussed later on in section 6. We would like to show here that, indeed, the angular cut-off comes out from the transfer matrix solution of the discretized RLC model. Moreover, our analysis will lead us to the formulation of a regularized version of the continuous RLC model.

Our procedure involves an analytic computation of the partial derivative with respect to k^2 of the transfer operator ground-state energy $\epsilon_0(\alpha,k^2)$, as defined by equation (32): $\partial_{k^2}\epsilon_0=(\partial\epsilon_0(\alpha,k^2)/\partial k^2)$. This derivative is very important physically, for the following two reasons. First, we remind that $\lim_{k^2\to 0}\partial_{k^2}\epsilon_0$ gives the second moment of the spontaneous "writhe" fluctuations $\langle{\chi_w}^2\rangle$ (see Eq. (24)), which was found to be infinite within the continuous RLC model. Second, for imaginary finite values of $k=i\kappa$, $\partial_{k^2}\epsilon_0$ enters in an essential way in the parametric representation of the extension *versus* supercoiling curves, to be derived in the next sections.

The partial derivative $\partial_{k^2}\epsilon_0$ is expressed, using equation (32), as

$$\frac{\partial\epsilon_0(\alpha,k^2)}{\partial k^2}=\frac{-A}{bt_0(\alpha,k^2)}\frac{\partial t_0(\alpha,k^2)}{\partial k^2}=\frac{-A}{bt_0(\alpha,k^2)}\left\langle t_0\left|\frac{\partial\hat{T}(\alpha,k^2)}{\partial k^2}\right|t_0\right\rangle.\quad(33)$$

The partial derivative with respect to k^2 of the transfer matrix $T(\theta_1, \theta_2, k^2)$ is easily obtained from equations (30) and (31):

$$\frac{\partial T(\theta_1,\theta_2,k^2)}{\partial k^2} = T(\theta_1,\theta_2,k^2)\mathcal{W}(\theta_1,\theta_2),$$
$$\mathcal{W}(\theta_1,\theta_2) = -\frac{1}{2}R(f(\theta_1,\theta_2,k^2))\frac{\left(1-\frac{\cos\theta_1+\cos\theta_2}{2}\right)^2}{f(\theta_1,\theta_2,k^2)}. \quad (34)$$

We have defined the small x cut-off function

$$R(x) = \frac{I_1(x)}{I_0(x)}, \quad (35)$$

which behaves like x when $x \ll 1$ and goes rapidly to 1 when $x > 1$. The next step is to investigate the variation of $T(\theta_1, \theta_2, k^2)$ as a function of $\Delta\theta = \theta_2 - \theta_1$ for a fixed value of $\theta = (\theta_1 + \theta_2)/2$, when $A/b \gg 1$. For the sake of simplicity we limit ourselves to a value of k^2 such that $|k^2|(b^2/A^2) \ll 1$, so that $f(\theta_1, \theta_2, k^2)$ can be approximated by $(A/b)\sin\theta_1 \sin\theta_2$. The transfer matrix is then given by the somewhat simplified expression

$$T(\theta_1,\theta_2,k^2) = \exp -\left\{\frac{A}{b}(1-\cos(\theta_1-\theta_2)) + \frac{b\alpha}{2A}(\cos\theta_1+\cos\theta_2)\right\} \times B_0\left(\frac{A}{b}\sin\theta_1\sin\theta_2\right), \quad (36)$$

where we have introduced the auxiliary function: $B_0(x) = \exp(-x)I_0(x)$ which is slowly varying with x: constant near the origin it behaves like $1/\sqrt{x}$ for large x. This formula shows that $T(\theta_1, \theta_2, k^2)$ is strongly peaked at small values of $|\Delta\theta|$, of order $\sqrt{b/A}$. This suggests the decomposition of $\mathcal{W}(\theta_1, \theta_2)$ as a sum of two terms involving a local potential $U_w(\theta)$ plus a small correction

$$\mathcal{W}(\theta_1,\theta_2) = (U_w(\theta_1)+U_w(\theta_2))/2 + \Delta\mathcal{W}(\theta_1,\theta_2), \quad (37)$$

$$U_w(\theta) = \mathcal{W}(\theta,\theta) = -\frac{b}{2A}R\left(\frac{A}{b}\sin^2\theta\right)\left(\frac{1-\cos\theta}{1+\cos\theta}\right). \quad (38)$$

A Taylor expansion of $\Delta\mathcal{W}(\theta_1, \theta_2)$ with respect to $\Delta\theta$, with θ kept fixed, gives $\Delta\mathcal{W} \propto \Delta\theta^2(1 + O(\Delta\theta^2))$. It confirms that the contribution of $\Delta\mathcal{W}$ relative to that of $\mathcal{W}$ is of the order of b/A. To be more quantitative, we have computed the two averages $\langle\mathcal{W}\rangle$ and $\langle\Delta\mathcal{W}\rangle$ using as weight function $T(\theta_1, \theta_2)\sin\theta_1 \sin\theta_2$. Taking $b = 0.14\,A$, we have obtained $|\langle\Delta\mathcal{W}\rangle/\langle\mathcal{W}\rangle| = 0.013$. It appears then quite legitimate to set $\Delta\mathcal{W} = 0$. This approximation allows us to write the partial derivative of the transfer operator $\hat{T}$ as a symmetrized operator product:

$$\frac{\partial\hat{T}(\alpha,k^2)}{\partial k^2} = \frac{\left(\hat{T}(\alpha,k^2)\hat{U}_w + \hat{U}_w\hat{T}(\alpha,k^2)\right)}{2}, \quad (39)$$

where $\hat{U}_w$ stands for the operator associated with the local potential $U_w(\theta)$.

Introducing this formula in equation (33) and remembering that $|t_0\rangle$ is an eigenstate of $\hat{T}$, the partial derivative $\epsilon_0(\alpha, k^2)$ takes the simple form

$$\frac{\partial\epsilon_0(\alpha,k^2)}{\partial k^2} = \frac{-A\langle t_0|\hat{T}\hat{U}_w + \hat{U}_w\hat{T}|t_0\rangle}{2t_0(\alpha,k^2)} = \frac{1}{2}\left\langle t_0\right|\left(\frac{1-\cos\theta}{1+\cos\theta}\right)R\left(\frac{A}{b}\sin^2\theta\right)\left|t_0\right\rangle. \quad (40)$$

The above result provides a very clear evidence that the discretization of the RLC model generates the angular cut-off around $\theta = \pi$ which we needed. Indeed, the integral involved in the above quantum average is now well defined for $\theta = \pi$, due to the the presence of the cut-off function $R(\frac{A}{b}\sin^2\theta)$.

Formula (40) leads in a natural way to a formulation of a regularized version of the continuous RLC model. The regularized operator Hamiltonian $\hat{H}^{\rm r}_{\rm RLC}$ is obtained from the Hamiltonian $\hat{H}_{\rm RLC}$ given in equation (20) by multiplying the singular "writhe" potential by the cut-off function $R((A/b)\sin^2\theta)$. Standard quantum mechanics rules applied to $\hat{H}^{\rm r}_{\rm RLC}$ give for $\partial_{k^2}\epsilon_0$ a formula identical to (40), provided it is legitimate to neglect the small difference between $|t_0\rangle$ and $|\Psi_0\rangle$, respectively, eigenstate of $\hat{T}$ and $\hat{H}^{\rm r}_{\rm RLC}(k)$. We have verified that it is indeed so by comparing the results obtained from the above regularized RLC continuous model and those given by the transfer matrix method: they do coincide to the level of few %, at least in the domain of stretching force explored in the present paper.

5 The RLC model for a quantitative analysis of supercoiled DNA stretching experiments

In this section we give the basic tools allowing to compute, within the RLC model, the various quantities measured experimentally.

We shall first study the "hat" curve which is a graph giving, for a given force F, the relative extension of molecule $\langle(z(L)/L)\rangle$ along the stretching force $\mathbf{F}$, as a function of the supercoiling angle $\chi = 2\pi n$. Figure 1 gives three examples of such "hat" curves taken within a rather large range of forces. The supercoiling angle is parameterized here by the ratio $\sigma = (n/L_{k0})$, where L_{k0} stands for the number of double-helix turns in the absence of external constraints. Positive values of σ correspond to overwinding, negative values correspond to underwinding. As is apparent in Figure 1, only the curve associated with a force of 0.2 pN looks really like a "hat". That is so for all the extension *versus* supercoiling curves taken in the force range $0.06\,\text{pN} \leq F \leq 0.45\,\text{pN}$. In contrast, when $F \geq 0.5\,\text{pN}$ a plateau develops in the underwinding region. This suggests that the torsional energy is converted into chemical energy instead of entropic elasticity energy. More precisely, convincing experimental arguments have been given [7,8] in favour of the following mechanism: the underwinding energy is used by the molecular system to

open the hydrogen bonds linking the bases and, as a consequence, denaturation bubbles appear along the DNA molecule. When the force is further increased, say above 3 pN, a plateau appears also in the overwinding region. This has received a very interesting interpretation [11] as a transition towards a new structure of the DNA: the so-called "P-DNA", which is also predicted by numerical simulations.

In the present paper, we shall focus our analysis on the true "hat" curves, *i.e.* those symmetric under the exchange $\sigma \Leftrightarrow -\sigma$, as observed for $F \leq 0.45$ pN.

5.1 The saddle point method

The experiments suggest that the variations of the relative elongation $\langle (z(L)/L) \rangle$ *versus* the supercoiling angle χ scale as a function of χ/L. It is convenient to introduce an intensive supercoiling variable $\eta = \chi A/L$ which will turn out to be at most of the order of few units in the domain we are going to explore. It is related to the usual variable σ by

$$\eta = \frac{\chi A}{L} = \frac{2\pi A}{p}\sigma = 94.8\sigma, \tag{41}$$

where we have used the values for the pitch $p = 3.4$ nm and the persistence length $A = 51.3$ nm.

Let us rewrite the partition function $Z(\chi, F)$ given by equation (22) in terms of scaling variables:

$$Z(\eta, \alpha) \simeq \int \mathrm{d}k \exp -\frac{L}{A}\left(\epsilon_0\big(k^2, \alpha\big) + \frac{k^2 A}{2C} - i\eta k\right). \tag{42}$$

The above partition function can be computed by the saddle point method in the limit $L/A \gg 1$ with η kept fixed. The saddle point is imaginary, $k_\mathrm{c} = i\kappa(\alpha)$ and is given by the equation

$$\frac{A}{C} + 2\frac{\partial \epsilon_0}{\partial k^2}(\alpha, -\kappa^2) = \frac{\eta}{\kappa}. \tag{43}$$

The saddle point contribution to the partition function $Z(\eta, \alpha)$ reads as follows:

$$\ln(Z(\eta, \alpha)) = -\frac{L}{A}\left(\epsilon_0(\alpha, -\kappa^2) - \frac{\kappa^2 A}{2C} + \eta\kappa\right) + O(1). \tag{44}$$

Let us first compute the torque Γ acting upon the free end of the molecule. The experiments to be analysed in this paper were not designed to measure Γ but there is an experimental project at ENS-Paris aiming at its direct empirical determination.

$$\frac{\Gamma}{k_\mathrm{B}T} = -\frac{\partial \ln Z}{\partial \chi} = -\frac{A}{L}\frac{\partial \ln Z}{\partial \eta} = \kappa + \frac{\partial \kappa}{\partial \eta}\left(\eta - \frac{\kappa A}{C} - 2\kappa\frac{\partial \epsilon_0}{\partial k^2}(\alpha, -\kappa^2)\right) = \kappa, \tag{45}$$

where the term proportional to $(\partial\kappa/\partial\eta)$ vanishes because of the saddle point equation (43). Therefore we have found that $\kappa = \Im(k_\mathrm{c})$ is equal to the torque Γ in units of $k_\mathrm{B}T$. One can introduce the thermodynamic potential $(\mathcal{G}/k_\mathrm{B}T) = -\ln(Z(\eta, u)) - \kappa\chi$ and verify that the supercoiling angle χ given by equation (43) satisfies the thermodynamic relation $\chi = -(\partial/\partial\kappa)(\mathcal{G}/k_\mathrm{B}T)$.

We are now going to compute in the same way the relative molecule elongation $\langle z(L)/L \rangle$:

$$\frac{\langle z(L) \rangle}{L} = \frac{k_\mathrm{B}T}{L}\frac{\partial \ln Z}{\partial F} = -\frac{\partial \epsilon_0(\alpha, -\kappa^2)}{\partial \alpha}. \tag{46}$$

As in the computation of the torque the term proportional to $\frac{\partial \kappa}{\partial \alpha}$ does not appear because it is multiplied by a factor which vanishes at the saddle point. In other words, the elongation is given by the same expression whether the experiment is performed under the conditions of fixed surpercoiling angle χ or fixed torque Γ. In contrast, the situation is very different for the elongation fluctuations: $\langle z(L)^2 \rangle - \langle z(L) \rangle^2$ turns out to be much larger if measured when the torque is kept fixed instead of the supercoiling angle, as we shall discuss later.

From the knowledge of $\epsilon_0(\alpha, -\kappa^2)$, using jointly equations (43) *and* (46) *one gets a parametric representation of the "hat" curves, the parameter being the torque in $k_\mathrm{B}T$ unit.*

5.2 Solving the quantum mechanics eigenvalues problems associated with the RLC model

In order to complete the description of the theory, we now sketch the methods used to get the final theoretical ingredients: the ground-state eigenvalue $\epsilon_0(\alpha, k^2)$ and its partial derivatives. We have followed two approaches.

5.2.1 Method a): Ground-state eigenvalue of the Hamiltonian $\hat{H}^\mathrm{r}_\mathrm{RLC}$ associated with the regularized continuous RLC model

In the first approach, the computations are performed within the continuous RLC model regularized according to the cut-off prescription derived in section 4.2. What we have to do is to solve the ground-state eigenvalue problem: $\hat{H}^\mathrm{r}_\mathrm{RLC}\Psi_0(\theta) = \epsilon_0\Psi_0(\theta)$. This ground-state wave function is obtained as an appropriate solution of the ordinary differential equation associated with the eigenvalue problem

$$\frac{1}{2\sin\theta}\frac{\partial}{\partial\theta}\left(\sin\theta\frac{\partial}{\partial\theta}\Psi_0(\theta)\right) + \big(-V_\mathrm{r}\big(\alpha, -\kappa^2\big) + \epsilon_0\big)\Psi_0(\theta) = 0, \tag{47}$$

where the regularized potential $V_\mathrm{r}(\alpha, k^2)$ is given by

$$V_\mathrm{r}(\alpha, k^2) = -\alpha\cos\theta + \frac{k^2}{2}\,\frac{1-\cos\theta}{1+\cos\theta}\,\frac{I_1(\frac{A}{b}\sin^2\theta)}{I_0(\frac{A}{b}\sin^2\theta)}. \tag{48}$$

We search for a solution which satisfies regularity conditions both for $\theta = 0$ and $\theta = \pi$. These requirements are

necessary and sufficient to guarantee that the differential operator $\hat{H}^{\rm r}_{\rm RLC}$ is a self-adjoint operator. They can be fulfilled if and only if the reduced energy ϵ belongs to a discrete set of values. As a first step, one constructs by series expansion two solutions of (47), $\Psi_a(\theta)$ and $\Psi_b(\theta)$, which are, respectively, regular for $\theta = 0$ and $\theta = \pi$. One then proceeds to an outward numerical integration of $\Psi_a(\theta)$ and inward numerical integration of $\Psi_b(\theta)$ up to an intermediate value of $\theta = \theta_0$. The energy eigenvalue equation is obtained as a matching condition for the two wave functions, which ensures the regularity of the eigenfunction for the whole physical domain of θ. One writes, for $\theta = \theta_0$, the equality of the logarithmic derivatives of $\Psi_a(\theta)$ and $\Psi_b(\theta)$

$$\frac{\partial \Psi_a}{\partial \theta}/\Psi_a - \frac{\partial \Psi_b}{\partial \theta}/\Psi_b = 0. \tag{49}$$

Equation (49) is then solved by a standard iteration method requiring a trial approximate eigenvalue. The construction of the parametric "hat" curve for a given value of α begins with a small value of κ (the energy $\epsilon_0(\alpha, 0)$ is easily obtained from the results of Ref. [10]). The trial eigenvalue needed to solve eigenvalue equation (47) for a small value of κ is easily obtained from a first-order perturbation calculation. Since the present method of solving the eigenvalue problem automatically yields the eigenfunction $\Psi_0(\theta)$, the partial derivatives of eigenvalues are readily obtained by taking the quantum average of the corresponding partial derivatives of the potential $V_{\rm r}(\alpha, k^2)$. Let us quote the derivative with respect to α (see Eq. (40) of section 4.2 for the derivative with respect to k^2)

$$\frac{\langle z(L)\rangle}{L} = -\frac{\partial \epsilon_0(\alpha, k^2)}{\partial \alpha} = \langle \Psi_0 | \cos\theta | \Psi_0 \rangle. \tag{50}$$

Once an eigenvalue is known for a value of k^2, one proceeds to the neighboring value $k^2 + \Delta k^2$, by using $\epsilon_0 + \Delta k^2 \frac{\partial \epsilon_0}{\partial k^2}$ as a trial eigenvalue and one proceeds to cover step by step the desired range of $k^2 = -\kappa^2$. The fact that the state found with this procedure is really the ground state can be checked from the fact that the wave function has no node.

5.2.2 Method b): The transfer matrix iteration

The search for the smallest eigenvalue $t_0(\alpha, k^2)$ of the transfer operator $\hat{T}(\alpha, k^2)$ defined by equations (29), (30) and (31) is done by iteration of the mapping $|z_n\rangle = \hat{T}|z_{n-1}\rangle$. Indeed, $|z_N\rangle = \hat{T}^N |z_0\rangle = \sum_n |t_n\rangle\langle t_n|z_0\rangle t_n^N$ is reduced to the lowest eigenvalue contribution when $N \to \infty$. Let us write the above mapping as a linear functional transform:

$$z_n(k, \theta_n) = \int_0^\pi \sin\theta_{n-1}\, {\rm d}\theta_{n-1} T(\theta_n, \theta_{n-1}) \times z_{n-1}(k, \theta_{n-1}). \tag{51}$$

In order to perform the integral over θ_{n-1}, we use the following discretization procedure. We divide the variation interval $0 \le \theta_{n-1} \le \pi$ into n_s segments $((s-1)\pi/n_s) \le \theta_{n-1} \le (s\pi/n_s)$. The integral over each segment is done with the standard Gauss method involving n_g abscissas and n_g attached weights. The integral over the full θ_{n-1} interval is then approximated by a discrete weighted sum over $d = n_s n_d$ points

$$\int_0^\pi f(\theta_{n-1}) \sin\theta_{n-1} {\rm d}\theta_{n-1} = \sum_{i=1}^{d} w_i \sin\theta_i f(\theta_i).$$

With the above integration procedure each iteration step can be reduced to a linear mapping in a d dimension Euclidean space $\mathcal{E}_d$. To each function $z_n(\theta)$ is attached a vector $\mathbf{Z}_n$ with d components $(\mathbf{Z}_n)_i = \sqrt{w_i \sin\theta_i} z_n(\theta_i)$. The additional factor has been introduced in such a way that the Hermitian norm $\langle z_n | z_n \rangle$ (defined from our discretized integration procedure) coincides with the Euclidian norm $\mathbf{Z}_n \cdot \mathbf{Z}_n$. The linear mapping in $\mathcal{E}_d$ is written as: $\mathbf{Z}_n = \mathcal{T}\mathbf{Z}_{n-1}$, where the elements of symmetric $d \times d$ matrix $\mathcal{T}$ are given by

$$(\mathcal{T})_{i,j} = \sqrt{w_i \sin\theta_i w_j \sin\theta_j}\, T\big(\alpha, k^2, \theta_i, \theta_j\big).$$

It is also easily verified that within our finite sum integration procedure we have $\langle z_n | \hat{T}(\alpha, k^2) | z_{n-1} \rangle = \mathbf{Z}_n \cdot \mathcal{T}\mathbf{Z}_{n-1}$. In order to give a simple criterion of convergence, it is convenient to require that at each iteration step the vector $\mathbf{Z}_n$ stays on the $\mathcal{E}_d$ unit sphere. This is achieved by using the following non-linear mapping:

$$\mathbf{Z}_n = \frac{\mathcal{T}\mathbf{Z}_{n-1}}{\sqrt{\mathbf{Z}_{n-1} \cdot \mathcal{T}^2 \mathbf{Z}_{n-1}}}. \tag{52}$$

The criterion of convergence is set up as follows:

Let us define $\Delta\mathbf{Z}_n = \mathbf{Z}_n - \mathbf{Z}_{n-\Delta n}$, where Δn is an integer, typically of the order of one hundred. $\mathbf{Z}_n$ is considered to be an appropriate fixed point $\mathbf{Z}_{\rm f}$ if $\sqrt{\Delta\mathbf{Z}_n \cdot \Delta\mathbf{Z}_n} \le \delta$. In practice we have taken $\delta = 10^{-4}$; this choice, together with $\Delta n = 200$, leads to a very tight convergence test.

Knowing $\mathbf{Z}_{\rm f}$ it is a straightforward matter to get the ground-state energy $\epsilon_0(\alpha, k^2)$ and its partial derivative with respect to α and k^2:

$$\begin{aligned}
\epsilon_0\big(\alpha, k^2\big) &= -\frac{A}{b} \ln t_0\big(\alpha, k^2\big) = -\frac{A}{b} \ln(\mathbf{Z}_{\rm f} \cdot \mathcal{T}\mathbf{Z}_{\rm f}), \\
\frac{\partial \epsilon_0(\alpha, k^2)}{\partial k^2} &= -\frac{A}{b t_0(\alpha, k^2)} \mathbf{Z}_{\rm f} \cdot \frac{\partial \mathcal{T}}{\partial k^2} \mathbf{Z}_{\rm f}, \\
\frac{\partial \epsilon_0(\alpha, k^2)}{\partial \alpha} &= -\frac{A}{b t_0(\alpha, k^2)} \mathbf{Z}_{\rm f} \cdot \frac{\partial \mathcal{T}}{\partial \alpha} \mathbf{Z}_{\rm f} = \mathbf{Z}_{\rm f} \cdot \mathcal{C}os \mathbf{Z}_{\rm f},
\end{aligned} \tag{53}$$

where the $\mathcal{C}os$ matrix elements are given by $(\mathcal{C}os)_{i,j} = \delta_{i,j} \cos\theta_i$.

It is also possible to get an explicit expression of the eigenfunction $\Psi_0(\theta)$ from the knowledge of the fixed point vector $\mathbf{Z}_{\rm f}$. The eigenfunction obeys the integral equation

$$\Psi_0(\theta) = \frac{1}{t_0} \int_0^\pi T(\theta, \theta_1) \Psi_0(\theta_1) \sin\theta_1 {\rm d}\theta_1. \tag{54}$$

Using our finite sum method to perform the integral over θ_1 in the r.h.s. of the above equation, $\Psi_0(\theta)$ is obtained immediately in terms of the components $Z_{\mathrm{f},i}$ of the fixed point vector

$$\Psi_0(\theta) = \frac{1}{t_0} \sum_i T(\theta, \theta_i) \sqrt{w_i \sin\theta_i} Z_{\mathrm{f},i}.$$

In our implementation of the method we have taken $n_g = 10$. The use of higher values of n_g may lead to overfitting. In contrast, we can vary more freely the number of sectors n_s. The ground-state energy $\epsilon_0(\alpha, k^2)$ and its partial derivatives vary by less than one part per million when n_s goes from 2 to 8 with $n_g = 10$. One has to go down to $n_g = 8$ and $n_s = 2$ to see a variation of about 10^{-5}. We have verified, using the high-precision integration subroutines provided by the Mathematica software, that the above wave function satisfies, in typical cases, the eigenvalue integral equation (54) to better than 10^{-9} with the choice $n_s = 4$ and $n_g = 10$.

The vector $\Delta\mathbf{Z}_n = \mathbf{Z}_n - \mathbf{Z}_{n-\Delta n}$ introduced to set up the convergence criterion can be used to get the energy ϵ_1 and the eigenfunction $\Psi_1(\theta)$ of the first excited state with a fairly good accuracy, say better than 10^{-3}. In particular the variation of the energy gap $\Delta\epsilon = \epsilon_1 - \epsilon_0$ *versus* η will shed some light upon the crossover phenomenon to be discussed in section 8.

6 Monte Carlo simulations with the discretized RLC model

The Monte Carlo procedure allows to generate configurations of the discretized RLC with a frequency proportional to their Boltzmann weight. A full simulation of the discrete model, incorporating the self-avoidance effects, the check that only unknotted configurations are kept, and the estimation of the writhe with the non-local Fuller formula was developed in [29] in the case of closed DNA chains. Vologodskii and Marko [30] were the first to adapt this formalism to the case of a single open supercoiled chain. In order to facilitate the transition from closed chain to open chain, they assume that the chain is confined between two impenetrable walls, with the two free ends sitting on different walls. From an experimental point of view, one wall is certainly welcome since in the actual experiments one molecule end is anchored by biochemical links to a glass plate. The other end is biochemically glued to a magnetic bead. In the experiments studied in this paper, the bead radius is one-seventh of the molecule contour length L, so that an unpenetrable wall looks somewhat inadequate to account for the geometrical obstruction of the magnetic bead, even if one neglects the very slow processes where the molecule releases the supercoiling by turning around the bead. The authors were, of course, aware of the problem and thus they limited their comparison to experiment to relative extension larger than 0.3. This wall effect is visible in the limit of zero supercoiling limit where the M.C. results differ significantly from the WLC at forces below 0.1 pN (in that case finite-size effects may also play a role since $L/A \sim 10$ to 20). If the two conditions $\langle z\rangle/L > 0.3$ and $F > 0.1$ pN are satisfied then a reasonable agreement was achieved with experiments over a rather broad range of forces and supercoiling. The agreement is particularly satisfactory for force extension curve at $\sigma = 0.031$ and this has allowed the authors to give an estimate of the twist rigidity C, with a 20% error bar. We shall return to this last point in section 7. Vologodskii and Marko have also investigated the effect of the reduced ioning strength which governs the DNA effective Coulomb radius, which can be characterized by the Debye length λ_{D}. Passing from 20 mN to 200 mN of NaCl leads to a Debye length reduction by factor $\sqrt{10}$. The calculated changes in the force extension curves at $\sigma = 0.01$ and $\sigma = 0.03$ are barely visible for stretching forces in the range $0.1\,\mathrm{pN} \leq F \leq 0.4\,\mathrm{pN}$. This includes the (F, σ) domain to be considered in the present paper. In the actual experiments, the Debye length corresponds to 30 mN of NaCl. Therefore the Vologodskii and Marko [30] findings suggest that the self-avoidance effects associated with the finite Coulomb radius play a relative minor role in the data to be analysed in the next section.

They present some evidence for the importance of knotting suppression in the particular case $F = 0.2$ pN and $\sigma = 0.05$. A typical simulated knotted configuration is seen to have the ability to absorb the supercoiling more efficiently than the corresponding unknotted one: it leaves the chain with a larger extension. Our analysis of the $F = 0.2$ pN hat curve of Figure 1 will concern the range $|\sigma| \leq 0.016$ which lies far away from the borderline point considered by the authors.

In the work presented here, we have performed a much less ambitious Monte Carlo simulation. We kept within the RLC model without self-avoidance, and the simulation was used essentially as a guide to validate our model, using the local formula for χ_W together with a discrete version of the chain: we checked that it is free of pathology and able to reproduce the experimental findings. It suggested to us that the length cut-off b provided by the elementary link of the discretized chain could generate the angular cut-off needed to regularize the continuous RLC model, as is shown in section 4.2. Our first computations within the regularized continuous model (the method a) of section 5.2.1) were checked on few points by Monte Carlo simulations and the agreement gave us confidence in our approach.

Subsequently we gave our preference to the transfer matrix iteration method of section 5.2.2 which uses exactly the same theoretical inputs as the Monte Carlo simulation but leads to accurate results with much less computer time. The fully discrete model involving three Euler angles per elementary link can be simulated, but it is more efficient for our purpose to make use of the fact that the ψ integrals can be done analytically, and thus to work only with the two angles θ and ϕ for each link. Indeed, using our computation of section 3 and integrating over the momentum k conjugate to the supercoiling angle χ after integrating out the ψ angles, the partition function of the

supercoiled DNA molecule can be written as

$$Z(\chi, F) = \int \mathcal{D}(\theta, \phi) \times \exp\left(- \frac{E_{\mathrm{WLC}}}{k_{\mathrm{B}}T} - \frac{C}{2L}\Big(\chi - \int \mathrm{d}s\dot{\phi}(1-\cos\theta)\Big)^2\right). \quad (55)$$

This is the path integral which we have discretized and simulated. The discretization procedure is exactly the one described in the previous section. We use N elementary links of length b, and the two discretization rules (25,26) for the energy function. The path integral measure is substituted by $\prod_{n=1}^{N} \mathrm{d}\phi_n \, \mathrm{d}\cos\theta_n$. The partition function is thus expressed as a $2N$-dimensional integral, and the corresponding probability measure can be sampled by Monte Carlo.

We use the standard Metropolis algorithm, where a new configuration of the chain is proposed at each step, the corresponding change of energy δE is computed, and the change is accepted with probability $\min(1, \exp(-\delta E/k_{\mathrm{B}}T))$. The point on which one must be careful is the choice of moves. Clearly, a choice of local moves (changing θ_n, ϕ_n on one link at a time) is a very bad one with which a macroscopic change of the molecule takes very many steps, and it leads to very long thermalization times. We have checked that it is in effect useless. We need to implement more sizeable moves, but moves which do not change the energy too much. One method which we have found rather effective is the following. We have first relaxed the constraint involving θ_N, which should not change the extensive properties of the chain. Then the moves consist in:

1) One picks up one link of the chain, number n.
2) One rotates the section of the chain $j \in n+1, \ldots, N$ by a global rotation. The rotation, of angle γ around an axis $\vec{n}$, is picked up at random, with a uniform distribution for the choice of $\vec{n}$ on the unit sphere, and a uniform distribution of γ on an interval $[-\delta, \delta]$ (a value of δ of order 0.5 is generally adequate).
3) One moves to the next link and iterates the procedure.

This is one of the types of moves which are used in the standard simulations of supercoiled DNA [29].

We have simulated mostly chains of 300 links, each link b having a length of one tenth of the persistence length. We have checked that the finite-size effects can be neglected with respect to the statistical errors for this value. For a given value of the supercoiling angle χ (or rather of its intensive version η), we perform a simulation, with a number of Monte Carlo steps per link of order 10^4. The first third of data is used for thermalization, the rest is used for measuring the distribution of elongation.

We show in Figure 2 the results for $\langle z \rangle / L$, and the statistical error bars. The computations were done at $C/A = 1.4$, and $b/A = 0.10$ for values of the force equal to 0.116 pN, and the amount of supercoiling given by $\eta = 0.0, 0.46, 0.92, 1.39$. We see that they are in rather good agreement with the experiment and the transfer matrix results. Note that since we do not have to use the two impenetrable walls trick, our computation is also valid in the zero supercoiling limit.

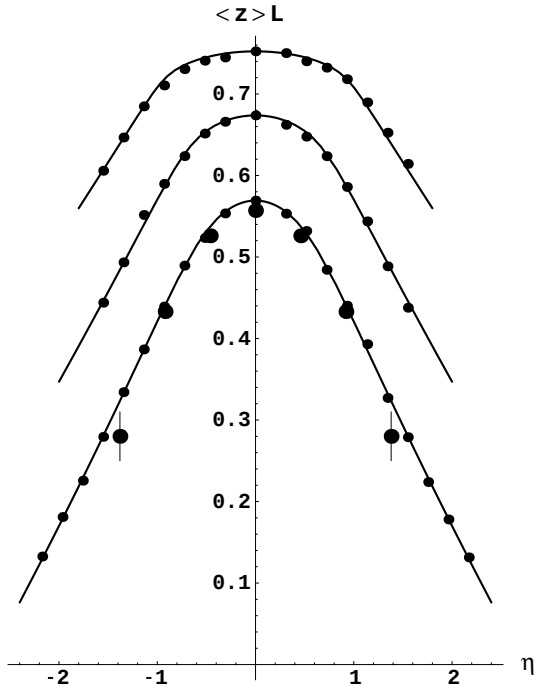

Fig. 2. The elongation *versus* reduced supercoiling angle, $\eta = 94.8\sigma$, for forces $F = 0.116$, 0.197, 0.328 pN, from bottom to top. The smaller points are the experimental results, the bigger points on the lowest curve are from Monte Carlo simulations and the full lines are the predictions of the RLC model obtained as indicated in the text.

When one increases the degree of supercoiling the thermalization time becomes prohibitive, and an examination of the configurations shows that they start building up some small fluctuating plectoneme-like structures. Clearly, in order to study this regime, one must first include self-avoidance, and then incorporate moves which are able to shift the plectonemes positions efficiently, as was done in [29,30]. We believe that this type of approach can be pursued further in order to get a precise comparison with experiments in the strongly supercoiled regime. It is complementary to the more restrictive, but more analytical, study at small supercoiling which we develop here.

7 Analysis of the experimental data on DNA extension versus supercoiling in the small force regime

In this section we are going to analyse a limited set of data obtained by the LPS-ENS group on the same single DNA molecule. They consist of three extension *versus* supercoiling curves with values of the stretching forces $F = 0.116$ pN, 0.197 pN and 0.328 pN. For these data a point-by-point evaluation of the systematic uncertainties is still lacking, so only the statistical uncertainties have been considered in the determination of the ratio $\frac{C}{A}$. A

simplified version of this analysis has been already given by us in a previous publication [12].

We have also performed two cuts upon the data in order to exclude from the analysis regions where the validity of RLC model is questionable. The first cut allows to neglect the effect of the plane onto which the DNA is attached. The second one allows to neglect the self-avoidance of the chain.

First we exclude values of the relative elongation such that $(\langle z(L)\rangle/L) \leq 0.1$. Experimentally, one end of the molecule is attached to a plane which thus implements a constraint $z(s) > 0$, for the whole chain. We shall see later on that when the reduced supercoiling parameter η increases from 0 to few units the probability distribution of θ develops a peak near $\theta = \pi$. Specially when $0 \leq (\langle z(L)\rangle/L) \leq 0.1$, it means that the RLC model is likely to generate configurations with $(z(s)/L) \leq 0$. We think that, for the experimental lengths L under study, the regime where $(\langle z(L)\rangle/L) > 0.1$ is such that, typically, the whole chain is in the half-plane $z > 0$.

The second cut excludes the too high values of the reduced supercoiling angle by imposing the condition $\eta \leq 1.5$ for $F = 0.197\,\mathrm{pN}$ and $F = 0.328\,\mathrm{pN}$. In a following section we shall present evidence that when $F = 0.328\,\mathrm{pN}$ the RLC model generates plectoneme-like configurations above a critical value $\eta_c \approx 1$. Our model ignores self-avoiding effects which are present under the actual experimental working conditions since the DNA Coulombic potential is only partially screened. The experimental plectonemes must have a radius[1] larger than the DNA Coulombic radius. In contrast, in the RLC model plectonemes with an arbitrary small radius can be generated. For a fixed variation of the supercoiling angle, the creation of a plectoneme, having a given length, absorbs on the average a smaller fraction of the DNA chain, in comparison with a situation where self-avoiding effects are involved. Indeed we have found that when the above constraints are not fulfilled the experimental points have a tendency to fall inside the theoretical hat curves, *i.e.* for a given η, experiment gives a smaller $\langle z(L)\rangle/L$.

In order to extract the values of C/A and of the cut-off b from the experimental data, we have used the following technique. Using equation (43) the ratio C/A can be written as a function of the reduced supercoiling angle η and the torque κ

$$\frac{A}{C} = \frac{\eta}{\kappa} - 2\frac{\partial \epsilon_0}{\partial k^2}(\alpha, -\kappa^2). \tag{56}$$

With the help of interpolation techniques, one can invert equation (46) in order to get κ as a function of $\langle z(L)\rangle/L$. In this way, each "hat" curve point of coordinates $(\eta, \langle z(L)\rangle/L)$ is associated with an empirical value of the rigidities ratio C/A, once a choice of the cut-off length b has been made. If the RLC model is to give a good representation of the data there must exist a value of b such that the empirical values C/A obtained from all points of all hat curves cluster around the correct result for C/A.

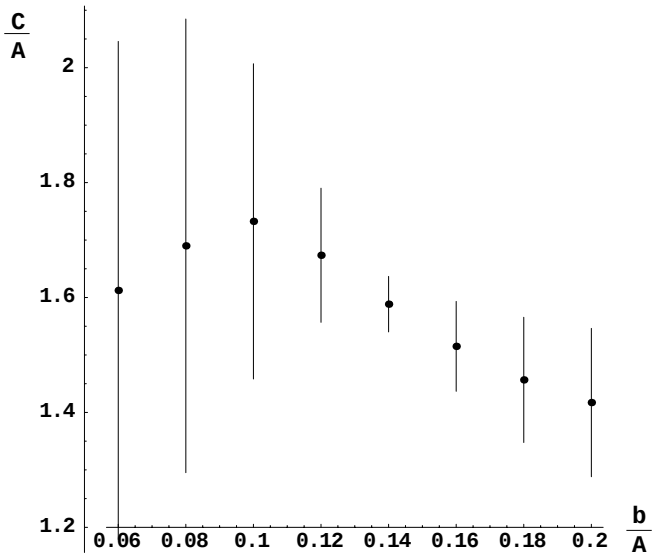

Fig. 3. Empirical determination of the cut-off length b and the ratio C/A from the hat curves analysis. In the case $F = 0.116\,\mathrm{pN}$, we have plotted, *versus* the cut-off b, the mean ratio $\langle C/A\rangle$ obtained by averaging the C/A values predicted by the RLC model from each empirical hat curve point. The error bar represents for each b the variance σ_r which leads to a measure of the RLC model ability to reproduce the hat curve data. A remarkable agreement is achieved with $b = 0.14\,A$ while it becomes very poor for $b = 0.06\,A$. This is consistent with the RLC model singularity near $b = 0$.

For $F = 0.116\,\mathrm{pN}$, we have plotted in Figure 3 the average ratio $\langle C/A\rangle$ and the variance $\sigma_r = \sqrt{\langle (C/A)^2\rangle - (\langle C/A\rangle)^2}$ *versus* the cut-off length b. The average and variance are computed over all the 20 experimental points of the hat curve. The point with $\eta = 0$ is an input, used to compute the dimensionless force parameter α. Using the scaling properties of the model, we have reduced the data analysis to a two-parameter fit: b/A and C/A. Since our model reduces to the WLC model in the $\eta = 0$ limit, it is legitimate to use the persistence length A obtained within the WLC model from the analysis of the force *versus* extension curve [10]. As is apparent in Figure 3, the RLC model with $b = 0.14\,A$ leads to a remarkably good agreement with the data. It corresponds to a minimum value of 0.03 of the quantity $(\sigma_r/\langle C/A\rangle)$ which measures the ability of our model to reproduce the data. The best cut-off length b value is approximately equal to twice the double-helix pitch. This is close to the length resolution Δl, which we had to invoke in order to justify the assumption of a cylindrically symmetric rigidity tensor. It is interesting also to note that the average value $\langle C/A\rangle$ *varies slowly with* b. The variance σ_r increases rapidly if one goes to small values of the cut-off length; this is consistent with the fact that the RLC model becomes singular in the limit $b \to 0$.

Similar results, somewhat less precise, have been obtained for the two other values of F considered in this

[1] The plectoneme radius is the common radius of the two interwound superhelices.

section. They favour the same value of b/A and give values of $\langle C/A\rangle$ consistent with the ones obtained for $F = 0.116\,\mathrm{pN}$, with variances σ_r about three times larger. Performing a weighted average upon the whole set of C/A empirical values obtained by the three hat curves, taking $b = 0.14\,A$, one gets the following empirical determination of the ratio of the two elastic rigidities involved in the RLC model

$$\frac{C}{A} = 1.64 \pm 0.04. \tag{57}$$

This result is in agreement with the value given in our previous work [12]: $(C/A) \simeq 1.68$. Since we have used data which do not incorporate in a quantitative way the systematic uncertainties, the above number should be considered as somewhat preliminary, but as it stands, it constitutes a significative improvement upon the previous empirical estimates.

We give in Figure 2 the theoretical "hat" curves using the ratio $(C/A) = \langle C/A\rangle$ obtained from the data at each force and the cut-off favored value $b = 0.14\,A$. The agreement with the experimental data is very satisfactory and confirms the overall consistency of the procedure. It should be stressed that the rather sharp bend connecting a slow quadratic decrease to a steep nearly linear falling down, which is observed for $\eta \simeq 1$ on the $F = 0.33\,\mathrm{pN}$ hat curve, is rather well reproduced by our model.

Using the values of the persistence length A obtained from the force *versus* extension curve measured on the same single molecule, one can obtain the following empirical value of the twist rigidity:

$$C = 84 \pm 10\,\mathrm{nm}. \tag{58}$$

The statistical error on C is of the order of 2 nm but the systematic errors are expected to be non-negligible and the overall uncertainty of 10 nm which accounts for those looks reasonable.

It is here of some interest to quote a recent empirical determination of the twist rigidity obtained from an analysis which does not involve the use of the RLC model or the like. A detailed account of the procedure is to be found in reference [9]. We shall here only quote the result: $C = 86 \pm 10\,\mathrm{nm}$, which is in good agreement with the number given by equation (58).

Vologodskii and Marko [30] have given previously an estimate of C obtained from one force extension curve at $\sigma = 0.031$, where the agreement with their Monte Carlo simulations is particularly striking: $C = 75 \pm 15\,\mathrm{nm}$. This result agrees with ours. Unfortunately they were not able to get any value of C, leading to an overall good fit for the complete set of force extension curves.

Moroz and Nelson [21,22] have analyzed the "hat" curves, using a perturbation approach to the RLC model. Because of the constraint $K = \sqrt{\alpha - (1/4)\kappa^2} > 3$, inherent to their method, they explore the force supercoiling angle domain given by $F \geq 0.3\,\mathrm{pN}$ and $\sigma \leq 0.01$. This implies that the ranges of relative extension for a given force are very narrow: for the top curve of Figure 2 ($F = 0.33\,\mathrm{pN}$): $0.72 \leq \langle z\rangle/L \leq 0.75$, the higher the force the narrower is the interval and closer to unity is its center. It is clear from Figure 2 that the range of relative extension analyzed in the present paper is much wider. In fact there is a rather small overlap of the experimental domains involved in the two analyses: the intersection of the two data sets amounts only to 20% of our present data set. Moroz and Nelson have incorporated hat curves data associated with relatively high force values: 0.6, 0.8, 1.3, 8.0 pN. For such forces, the RLC model is certainly not valid when $\sigma < 0$ and even for $\sigma > 0$ in the case of the highest force. They [22] have derived from their two-parameter fit (A, C) the twist rigidity value $C = 109\,\mathrm{nm}$ (in a preliminary analysis [21] based upon a more limited set of data they gave $C = 120\,\mathrm{nm}$). These authors did not give the uncertainty associated with C and the value of A coming out from their two-parameter fit. Because of the limited range of relative extension values they can fit, we believe that the error bars on their results should be larger than ours. As a comparison, we have used $C = 109\,\mathrm{nm}$ to compute the theoretical hat curves of Figure 2. As expected, the quality of the fit becomes significantly poorer: the overall χ_2 is multiplied by 5.3 when one goes from $C = 86\,\mathrm{nm}$ to $C = 109\,\mathrm{nm}$.

8 Twist, writhe and plectonemes

In this section we would like to use our solution of the discretized RLC model to study, at a given force ($F = 0.33\,\mathrm{pN}$), the variations of the torque, twist and writhe thermal averages *versus* the supercoiling reduced angle η. As we shall see, there exist two very different regimes. Below a rather sharply defined value of the supercoiling angle η_c, the DNA chain behaves nearly as an elastic non-flexible rod. Above η_c the torque becomes nearly independent of supercoiling while the writhe grows linearly with it. We shall give arguments suggesting that in the high η regime the supercoiling constraint is satisfied by the creation of plectoneme-like configurations.

8.1 Relation between the torque and the average twist

To begin, we are going to prove that the thermal average of the rod twist $\langle T_w\rangle$ is given in terms of the torque Γ by the classical elasticity formula for a non-flexible rod:

$$\langle T_w\rangle = \frac{\kappa L}{C} = \frac{\Gamma L}{\mathcal{C}}, \tag{59}$$

where $\mathcal{C} = k_\mathrm{B}TC$ is the usual twist rigidity. It is convenient to introduce the joint probability distribution of a DNA chain configuration $\mathcal{P}(\chi_1, \chi_2)$ with $T_W = \chi_1$ and $\chi_W = \chi_2$; it can be written as the double Fourier transform:

$$\mathcal{P}(\chi_1, \chi_2) \propto Z(\chi_1, \chi_2) = \int \frac{\mathrm{d}k_1\,\mathrm{d}k_2}{4\pi^2} \exp(-ik_1\chi_1 - ik_2\chi_2)\tilde{Z}(k_1, k_2),$$

where $\tilde{Z}(k_1, k_2)$ is given by the functional integrals

$$\tilde{Z}(k_1,k_2) = \int \mathcal{D}(\theta,\phi) \exp\left(ik_2\chi_W - \frac{\mathcal{E}_{\text{bend}} + \mathcal{E}_{\text{stretch}}}{k_{\text{B}}T} \right) \times \tilde{Z}_T(k_1),$$

$$\tilde{Z}_T(k_1) = \int \mathcal{D}(\psi) \exp\left(ik_1 T_w - \frac{\mathcal{E}_{\text{twist}}}{k_{\text{B}}T} \right).$$

As in section 3.2, we perform explicitly the functional integral upon ψ and get $\tilde{Z}_T(k_1) = \exp(-k_1^2 L/2C)$. This leads to the factorization property $\tilde{Z}(k_1,k_2) = \tilde{Z}_T(k_1)\tilde{Z}_W(k_2)$, where the writhe term $\tilde{Z}_W(k_2)$ is given by the path integral

$$\tilde{Z}_W(k) = \int \mathcal{D}(\theta,\phi) \exp\left(ik\chi_W - \frac{E_{WLC}}{k_{\text{B}}T} \right).$$

As a physical consequence, the twist T_w and the writhe χ_W fluctuate independently in the RLC model, when no supercoiling constraint is applied upon the free end of the molecule.

The thermal average $\langle T_w \rangle$, in the presence of the supercoiling constraint $\chi = T_w + \chi_W$, is then given by

$$\langle T_w \rangle = \frac{1}{Z(\chi,F)} \int \mathrm{d}\chi_1\, \mathrm{d}\chi_2 \chi_1 Z_T(\chi_1) Z_W(\chi_2) \times \delta(\chi_1 + \chi_2 - \chi) = \frac{1}{Z(\chi,F)} \int \frac{\mathrm{d}k}{2\pi} \left(-i \frac{\mathrm{d}\tilde{Z}_T}{\mathrm{d}k} \right) \tilde{Z}_W(k) \exp(-ik\chi).$$

Using the explicit form of $\tilde{Z}_T$, one gets the announced formula and by subtraction the writhe thermal average

$$\langle T_w \rangle = -\frac{L}{C} \frac{\partial \ln Z}{\partial \chi} = \frac{L}{C} \frac{\Gamma}{k_{\text{B}}T},$$

$$\langle \chi_W \rangle = \chi - \langle T_w \rangle = \frac{2L\kappa}{A} \frac{\partial \epsilon_0(\alpha, -\kappa^2)}{\partial k^2}. \quad (60)$$

8.2 The average writhe in the zero stretching force limit: a comparison with Monte Carlo simulations of self-avoiding closed supercoiled DNA chains

The above formulas offer the opportunity to compare the RLC model predictions with closed DNA chain Monte Carlo simulations [29], which incorporate self-avoiding effects. Using the same ratio $C/A = 1.5$ and the same value of $b/A = 0.2$ as Vologodskii *et al.* [29], we have computed $\lim_{F=0}\langle \chi_W \rangle/\chi = \langle Wr/\Delta Lk \rangle$ for σ values taken in the range $0 \leq -\sigma \leq 0.04$. The comparison with the numbers taken from reference [29] is displayed in Figure 4. It is apparent that the RLC model computations, and Monte Carlo simulations are in rather good agreement: when $|\sigma| \leq 0.02$—the range explored in our previous data analysis—the results diverge by less than 8.5% and the difference reaches 10% when $|\sigma| \to 0.04$. They both agree rather well with the measurements performed in references [26] and [27]. If we forget about the possible finite-size effects in the Monte Carlo simulations where $A/L \simeq 1/12$, the small deviation may tentatively be attributed to the self-avoiding effects not incorporated in our computations.

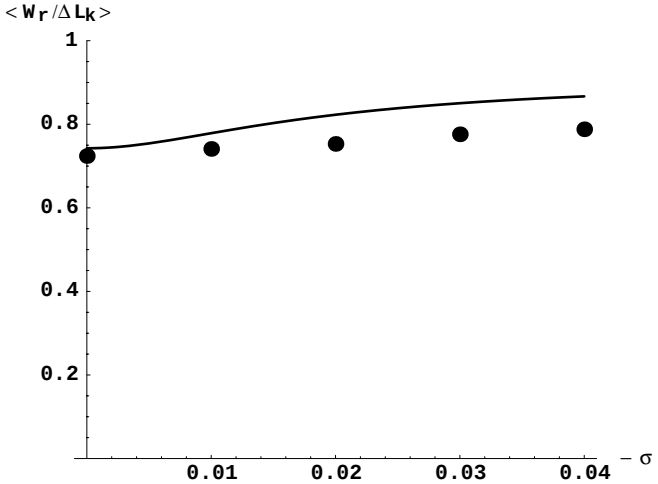

Fig. 4. Comparison of Monte Carlo (●) and the RLC model (continuous line) results for the reduced average $\langle Wr/\Delta Lk \rangle = \lim_{F=0}\langle \chi_W \rangle/\chi$.

8.3 A torque and writhe versus supercoiling cross-over: a possible sign for thermal excitation of plectoneme-like configurations

In Figure 5 we have plotted (for the case $F = 0.33\,\text{pN}$) the torque in $k_{\text{B}}T$ unit, κ, together with the ratio of writhe to twist χ_W/T_w as functions of the scaled supercoiling variable $\eta = (\chi A/L)$. These theoretical curves have been obtained with the same parameters as the "hat" curves of Figure 2. They show a very rapid change of behaviour, a quasi-transition, for $\eta_{\text{c}} \approx 1.0$, with the following two very different regimes:

- Below η_{c} the twist of the DNA chain increases linearly with the supercoiling η, as in a non-flexible rod with an effective twist rigidity $C_{\text{eff}} = 0.82C$. The ratio of writhe to twist stays almost constant at the value 0.2.
- Above η_{c} the torque depends weakly on the supercoiling η, the twist becomes nearly constant while the writhe increases linearly with the supercoiling.

The behaviour in the large supercoiling regime is reminiscent of the mechanical instability leading to the formation of plectonemes which is easily observed by manipulating macroscopic elastic rods such as telephone cords. One must be careful with this analogy because the plectonemic instability corresponds to a zero temperature limit, while in the case of DNA, much of the elasticity comes from entropic effects and thermal fluctuations play a crucial role [17]. Yet we would like to point towards the existence, in the large supercoiling regime of the RLC, of excitations which share some of the properties of plectonemes.

We define $\mathcal{E}_p$ as a set of undeformed plectonemes having the axis of their winding *helices arbitrarily oriented with respect to the force direction* (z-axis). We then introduce the angular distribution $P(\theta)$ of the tangent vector $\hat{\mathbf{t}}$ about the z-axis, averaged along the plectoneme and upon the set $\mathcal{E}_p$. Let us sketch the proof of the symmetry relation: $P(\theta) = P(\pi - \theta)$. Introducing the angular distribution $\mathcal{P}(\alpha_p)$ of the plectonemes axis and the tangent vector $\hat{\mathbf{t}}_{\rm plect}(s)$ relative to a vertical plectoneme, $P(\theta)$ reads as follows:

$$P(\theta) = \int_0^\pi \mathcal{P}(\alpha_p)\,\mathrm{d}\alpha_p \frac{1}{L} \times \int_0^L \mathrm{d}s\,\delta\big(\cos\theta - \hat{\mathbf{z}}\cdot R(\hat{\mathbf{y}},\alpha_p)\hat{\mathbf{t}}_{\rm plect}(s)\big).$$

Ignoring the plectoneme handle contribution, we can rewrite $P(\theta)$ in terms of the vertical solenoid ϕ-dependent tangent vector $\hat{\mathbf{t}}_{\rm sol}(\phi,\theta_0) = R(\hat{\mathbf{z}},\phi)R(\hat{\mathbf{y}},\theta_0)\hat{\mathbf{z}}$:

$$P(\theta) = \int_0^\pi \mathcal{P}(\alpha_p)\,\mathrm{d}\alpha_p \frac{1}{4n_0\pi} \times \int_0^{2n_0\pi} \mathrm{d}\phi\big(\delta(\cos\theta - \hat{\mathbf{u}}(\alpha_p)\cdot\hat{\mathbf{t}}_{\rm sol}(\phi,\theta_0)\big) + (\phi\to\pi-\phi,\theta_0\to\pi-\theta_0)),$$

where we have used the idendity $\mathbf{A}\cdot R\mathbf{B} = R^{-1}\mathbf{A}\cdot\mathbf{B}$ and defined the unit vector $\hat{\mathbf{u}}(\alpha_p) = R(\hat{\mathbf{y}},-\alpha_p)\hat{\mathbf{z}}$. Then we compute $\hat{\mathbf{u}}(\alpha_p)\cdot\hat{\mathbf{t}}_{\rm sol}(\phi,\theta_0) = \sin\alpha_p\cos\phi\sin\theta_0 + \cos\alpha_p\cos\theta_0$ and by simple inspection we arrive at the desired relation. Because of the ϕ averaging, the proof holds true if one takes an arbitrary axis in the $z=0$ plane instead of the y-axis to rotate the plectoneme. In practice the plectonemes are deformed by the thermal Brownian motion. More complex structures can also appear, like branched plectonemes. It looks, however, reasonable to assume that the above symmetry property is not affected, on average, by thermal fluctuations.

In order to measure the degree of symmetry of the distribution of θ angle along the chain, we introduce the function *plecto*(η) defined as follows:

$$plecto(\eta) = \frac{\int_0^\pi P(\theta,\eta)P(\pi-\theta,\eta)\,\mathrm{d}(\cos\theta)}{\int_0^\pi P(\theta,\eta)^2\,\mathrm{d}(\cos\theta)}. \qquad (61)$$

It is clear that *plecto*(η) reduces to unity for pure plectonemic configurations and goes to zero in the limit of rectilinear chains. Within the RLC model, the probability $P(\theta,\eta)$ is given by the thermal average of the molecular axis angular distribution when one runs along the molecular chain. Exploiting the quantum mechanics analogy, it is easily proved that $P(\theta,\eta)$ is equal to $\Psi_0(\theta)^2$, the square of the ground-state wave function introduced in section 5.2. This has been used to compute the function *plecto*(η) which is plotted in Figure 5. The shape of $P(\theta,\eta)$ changes in a very characteristic way when one goes from $\eta = 0$ to $\eta \approx 4$. When $0 \le \eta \le \eta_c \approx 1$, $P(\theta,\eta)$ has a rather narrow peak at $\theta = 0$ with a nearly vanishing tail for $\theta > \frac{\pi}{2}$. As a consequence, the function *plecto*(η) is practically null within this interval. A secondary peak at $\theta = \pi$ begins to develop when $\eta \ge \eta_c$ and it reaches about the same height as the primary peak at $\eta \approx 4$. The building of this two-bump structure is accompanied by an almost linear increase of the function *plecto*(η) which reaches the value 0.9 near $\eta = 4$. This behaviour suggests that thermally deformed plectoneme-like configurations are responsible for the sharp increase of the writhe-to-twist ratio and the flattening of the curve torque *versus* supercoiling above the critical value $\eta_c \approx 1$. Finally a useful piece of information about the quasi-transition near $\eta \ge \eta_c$ is the study of the variation of the energy gap between the ground state and the first excited state $\Delta\epsilon = \epsilon_1 - \epsilon_0$, obtained by the method given in section 5.2.2. The corresponding curve appears in Figure 5 under the label "Gap". $\Delta\epsilon$ is a decreasing function of η, with a rather sudden fall near $\eta \approx \eta_c$. This somewhat technical feature has a nice physical interpretation in terms of the correlation length associated with the $\cos\theta$ fluctuations, *at fixed torque*, which is given by $A/\Delta\epsilon$. The jump of this correlation length around η_c is a further sign of a fast change of physical regime.

The two regimes of supercoiling displayed on Figure 5 are related, within the quantum mechanical formalism of section 5.2.1, to the double-well structure of the potential

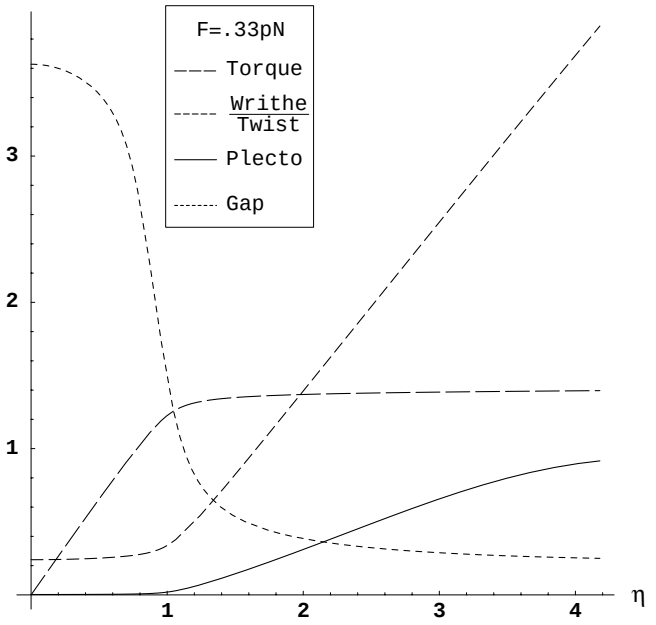

Fig. 5. Twist, writhe and plectonemes in the RLC model. We display several curves which indicate that a cross-over phenomena is taking place near $\eta_c \approx 1$. After a linear increase, expected for a non-flexible rod, the torque becomes independent of the supercoiling above η_c. Simultaneously, the writhe-to-twist ratio, which was staying constant around 0.2, starts a rather steep linear increase. Near η_c the function *plecto*(η), which measures the forward backward symmetry of the $\hat{\mathbf{t}}$ angular distribution relative to $\mathbf{F}$, takes off from 0 to the value 0.9. (*plecto* = 1 for a plectonemic configuration). All these features suggest that the cross-over could be attributed to the creation of plectoneme-like configurations.

$V_{\rm r}(\alpha, k^2, \theta)$ when $k^2 = -\kappa^2$. On the one hand, the potential has a relatively shallow well at $\theta = 0$, associated with the stretching potential energy. On the other hand, the regularized "writhe" potential produces a deep narrow hole at $\theta = \pi$. Let us call ϵ_a, Ψ_a and ϵ_b, Ψ_b the eigenvalues and eigenstates associated, respectively, with the semiclassical states localized in the two potential wells. As κ is increasing, the energy levels ϵ_a and ϵ_b are approaching each other. The level crossing is avoided near $\kappa_{\rm c}$ by a quantum tunneling through the finite height wall between the two wells. This accounts for the peculiar variation of $\Delta\epsilon$ near $\eta_{\rm c}$. The mixing of the two levels Ψ_a and Ψ_b by quantum tunnelling generates the secondary bump in the probability distribution $P(\theta)$. In the vicinity of the near crossing point, the ground-state energy ϵ_0 depends almost linearly upon the tunneling amplitude t_{ab}, which has typically a very rapid variation with κ^2. Since the ratio η/κ is a linear function of $(\partial\epsilon_0/\partial\kappa^2)$ (see Eq. (43)), η should exhibit a very sharp increase with $\kappa \geq \kappa_{\rm c} \approx 1.4$ as is easily seen by turning Figure 5 by 90 degrees.

9 Fluctuations of the extension in a supercoiled DNA molecule

In this section we would like to give a brief analysis of preliminary measurements of the supercoiled DNA extension fluctuations, performed at a force $F = 0.33\,\mathrm{pN}$ by the experimental group in the ENS. We shall compare the experimental results with the RLC model predictions using the parameters b/A and C/A deduced from the extension *versus* supercoiling curves analysis, performed in section 7. The mean-square deviations of the fluctuations of the molecule extension along the force direction is given by the second derivative of the free energy $\mathcal{F} = -k_{\rm B}T \log Z(F)$ with respect to F:

$$\left\langle \delta z^2 \right\rangle = \left\langle z^2 \right\rangle - \left\langle z \right\rangle^2 = (k_{\rm B}T)^2 \frac{\partial^2 \log Z}{\partial F^2}. \qquad (62)$$

It is convenient to replace the first derivative $(\partial \log Z/\partial F)$ by its expression in terms of the average relative extension using equation (46). The extension mean-square fluctuation can then be written as follows:

$$\left\langle \delta z^2 \right\rangle = L\left(\frac{k_{\rm B}T}{F}\right)\alpha\frac{\partial}{\partial\alpha}\left(\frac{\langle z\rangle}{L}\right). \qquad (63)$$

We have verified that the value of $\langle \delta z^2 \rangle$ obtained in the discretized RLC model in the limit of no supercoiling, $\chi = 0$, agrees with the one given by the WLC model to better than $3 \cdot 10^{-3}$. In the situation where the free end of the molecular chain is subjected to a supercoiling constraint the fluctuations will be different depending on whether the measurement is performed at fixed torque κ or at fixed supercoiling angle χ. In the first case the result is readily obtained from equation (46):

$$\left\langle \delta z^2 \right\rangle|_\kappa = -L\left(\frac{k_{\rm B}T}{F}\right)\frac{\alpha\partial^2\epsilon_0(\alpha,-\kappa^2)}{\partial\alpha^2}. \qquad (64)$$

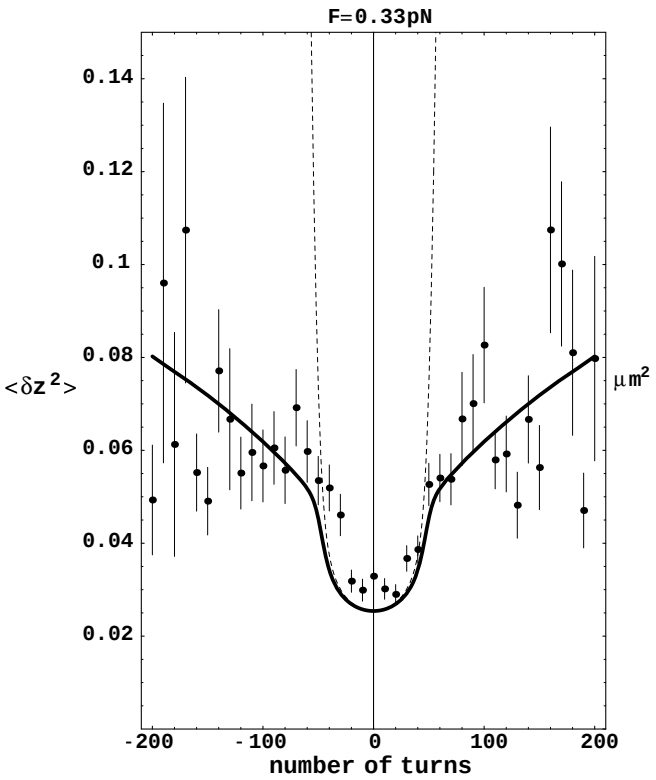

Fig. 6. Mean square fluctuations of DNA supercoiled molecule extension for $F = 0.33\,\mathrm{pN}$. The points are the experimental data. The thick continuous line is the theory, for the experimental situation where the supercoiling turn number $n = (L\eta/2\pi A) \approx 50\eta$ is fixed. The dotted line is the theoretical result for another situation where the torque would be fixed (the number of turns is then to be understood as a thermal average value).

In the actual experiment the extension fluctuations are measured at fixed χ and an extra term has to be added to the above expression due to the fact that the torque is now a function of α and η:

$$\left\langle \delta z^2 \right\rangle|_\eta = L\left(\frac{k_{\rm B}T}{F}\right)\alpha\Bigg(-\frac{\partial^2\epsilon_0(\alpha,-\kappa^2)}{\partial\alpha^2} + 2\kappa\frac{\partial\kappa}{\partial\alpha}\frac{\partial^2\epsilon_0(\alpha,-\kappa^2)}{\partial\alpha\partial k^2}\Bigg). \qquad (65)$$

Using equation (43), the extra term can be transformed by writing $2(\partial\epsilon_0/\partial k^2)(\alpha,-\kappa^2) = \frac{\eta}{\kappa} - A/C$. One gets finally the mean square extension fluctuations at fixed supercoiling angle

$$\left\langle \delta z^2 \right\rangle|_\eta = \left\langle \delta z^2 \right\rangle\big|_\kappa - L\left(\frac{k_{\rm B}T}{F}\right)\alpha\frac{\eta}{\kappa}\left(\frac{\partial\kappa}{\partial\alpha}\right)^2. \qquad (66)$$

In the above formula the second term is clearly negative so we expect that $\langle \delta z^2 \rangle|_\eta < \langle \delta z^2 \rangle|_\kappa$. The curves giving $\langle \delta z^2 \rangle$ *versus* the number of supercoils $n = (L\eta/2\pi A) \approx 50\eta$ are displayed in Figure 6, $\langle \delta z^2 \rangle|_\eta$ as a thick continuous

line and $\langle \delta z^2 \rangle|_\kappa$ as a dashed line. It appears clearly that $\langle \delta z^2 \rangle|_\eta \ll \langle \delta z^2 \rangle|_\kappa$, when $|\eta| > \eta_c \approx 1$. This implies a strong cancellation between the two terms of formula (66), which is then not suitable for an evaluation of $\langle \delta z^2 \rangle|_\eta$. To get the thick solid curve of Figure 6, we have used the fact that the calculation procedure giving, at reduced force α, the relative extension *versus* the supercoiling angle, $(\langle z \rangle / L)(\alpha, \eta)$, is precise enough to allow the evaluation of the partial derivative with respect to α by a three-point finite-difference formula.

The difference between the two statistical ensembles can be understood qualitatively from the previous section considerations and specially by looking at the curves of Figure 5. In a situation where the torque is fixed at $\kappa = \kappa_c \approx 1.4$ the supercoiling angle χ is practically unconstrained. It can fluctuate rather freely through thermal excitation of plectonemes, which have no effect upon the torque. In contrast when η is fixed at a value $\eta > \eta_c \approx 1$ the ensemble is more constrained. The torque κ is still practically fixed at the critical value κ_c. As a consequence, the writhe $\chi_W = \chi - T_w \approx \chi - \kappa_c L/C$ has approximately a fixed value and then the only plectonemes which can be created are those having a very limited range of writhe.

As is apparent in Figure 6, the experimental points agree reasonably well with the RLC model predictions, taking into account the quoted uncertainties, which are exclusively of statistical origin. (Systematic effects are smaller.) We notice the quasi-critical jump of $\langle \delta z^2 \rangle|_n$, near $n_c \approx 50$, which is also present in the data.

10 Summary and conclusion

Together with new relevant contributions, this paper gives a detailed account of a work of the authors, which appeared previously under a very concise letter form [12]. It was a rather successful attempt to describe the entropic elasticity of supercoiled single DNA molecule in terms of the thermal fluctuations of an elastic rod.

As in most works based upon a similar model, the rigidity tensor was assumed to be symmetric under rotations about the molecular axis and then fully described by two elastic constants, the bending and twist rigidities. Because of the DNA helical structure, one may have expected an axially asymmetric rigidity tensor, involving extra elastic constants. We have proved in this paper that axial symmetry breaking contributions to the elastic energy are averaged out upon a "coarse graining" involving a length resolution Δl about three times the double-helix pitch p. Such a value corresponds to the actual experimental resolution. The model developed in the present paper is not expected to be realistic at length scale below twice the DNA double-helix pitch.

To implement in the RLC partition function the supercoiling empirical constraint χ, we have followed a direct procedure, instead of adapting to open molecular DNA chains the formalism used in the study of supercoiled plasmids. Imposing a well-defined regularity condition upon the Euler angles describing locally the molecular chain, we have been able to decompose the empirical supercoiling angle χ as a sum of two line integrals T_w and χ_W, associated, respectively, with the twist and writhe contributions. The local writhe χ_W is a line integral taken along regular trajectories of the chain unit tangent vector $\hat{\mathbf{t}}$. They are drawn upon the unit sphere S_2 pierced by a hole having a small radius ϵ, localized at the south pole defined by the stretching force direction. Such a prescription forbids the crossing of a spherical coordinate singularity which would invalidate our derivation of the local writhe formula. When it is applied in compliance with the above prescription, the local writhe formula allows correct evaluations of the writhe of solenoid and plectoneme configurations, having an arbitrarily space orientation. More generally the local writhe formula, though not explicitly rotation invariant, is shown to lead, in the small ϵ limit, to rotation invariant results.

The partition function of the RLC having a given supercoiling angle χ is written as the convolution product of the partition function $Z_T(T_w)$ of a twisted non-flexible rod times the partition function $Z_W(\chi_W)$ of a worm-like chain having a fixed writhe angle. The Fourier transform $\tilde{Z}_W(k)$ is shown to be the analytic continuation to imaginary time of the Feynman amplitude describing the quantum evolution of unit charge particle moving upon a sphere upon the joint action of an electric d.c. field and a magnetic monopole having an unquantized charge k. The associated Hamiltonian $\hat{H}_{\mathrm{RLC}}(k)$ is readily obtained from standard quantum mechanics rules.

As in the quantum magnetic monopole problem, we have found a pathology which is associated with the singular behaviour of the $\hat{H}_{\mathrm{RLC}}(k)$ potential term near the south pole. We have proved that an angular cut-off is generated by a discretization of the chain involving an elementary link b (this result was given without proof in our previous work [12]). We have derived analytically from the discretized elastic energy a regularized version of RLC continuous model. The singular writhe potential is multiplied by a regulating function going smoothly to zero when $\sin^2\theta \leq (b/A)$. We have arrived in this way at a well-behaved Hamiltonian $\hat{H}^{\mathrm{r}}_{\mathrm{RLC}}(k)$, which provided a precise mathematical definition of RLC model used in this paper. It leads to a partition function free of any pathology. In an independent work following ours [12], Moroz and Nelson proposed a high force perturbation method [21], where no angular cut-off is introduced from the start. To finite order, the divergent perturbation series, hopefully asymptotic, does not see the singularity at the south pole, though it is always present in the model. In order to make contact with experiment, the authors have to impose upon their expansion parameter a sharp "technical" bound. Its effect is to restrict considerably the domain of force and supercoiling where a comparison with experiment is possible. This limits the precision of their determination of C.

Within our regularized RLC model, we have developed methods allowing the computation, to an arbitrary precision, of the relative extension *versus* supercoiling curves, the so-called "hat" curves. The Fourier transform involved in the partition function is evaluated by the saddle point

method, in the limit of a contour length L much larger than the persistence length A. It leads to a parametric representation of the hat curves in terms of the torque acting upon the molecule's free end. The final theoretical ingredient is the ground-state energy of the regulated RLC Hamiltonian. It is obtained following two methods: a) an explicit solution of the Schrödinger equation associated with $\hat{H}^{\mathrm{r}}_{\mathrm{RLC}}(k)$, b) the iteration of the transfer matrix deduced directly from the discretized elastic energy. Though they are not strictly equivalent from a mathematical point, they lead to identical results to few %.

Our data analysis involves three values of the stretching forces: $F = 0.116$, 0.197, $0.328\,\mathrm{pN}$. For each hat curve point and a fixed (b/A), the RLC model leads to an empirical value of the ratio C/A as a function of the measured relative extension and supercoiling angle. If the model provides an adequate description of the hat curve, the set of empirical values should cluster around the actual value C/A. For each cluster we have plotted the mean value $\langle C/A\rangle$ and the variance σ_{r} *versus* b/A. The best value $b/A = 0.14$ corresponds to the minimum of the ratio $\sigma_{\mathrm{r}}/\langle C/A\rangle$, which measures the ability of the model to fit the data. The preferred cut-off length b is found to be about two times the double-helix pitch and it is close to the length resolution Δl invoked to suppress axially asymmetric elastic energy terms. Our determination of $C/A = 1.64 \pm 0.04$ is obtained from a weighted average of $\langle C/A\rangle$ relative to the three forces involved in the fit, taking $b/A = 0.14$. This number turns out to be remarkably stable under variations of b within the range $0.08\,A \leq b \leq 0.2\,A$: the deviations of C/A from 1.64 stay below the level of 8%. In contrast, the quality of the hat curves fit which is very satisfactory at the best b value becomes poorer away from it, specially for low b values. Our central value for the twist rigidity $C = 84 \pm 10\,\mathrm{nm}$ differs by about 25% from the ones given by Moroz and Nelson [22]. The absence of any uncertainty estimate and an analyzed data set having a small overlap with ours makes the physical significance of this apparent discrepancy difficult to assess.

Although these quantities are not yet directly accessible to experiment, we have computed, as functions of the supercoiling χ, the torque Γ and the average twist $\langle T_w\rangle$ (or equivalently the average writhe $\langle \chi_W\rangle = \chi - \langle T_w\rangle$). Use has been made of a remarkable property: $\langle T_w\rangle$ is related to Γ by the linear elasticity formula for a non-flexible twisted rod.

In the case of the highest force ($F = 0.33\,\mathrm{pN}$), the two curves, torque and writhe-to-twist ratio *versus* supercoiling, exhibit a rather sharp change of regime near the same critical value χ_{c} of the supercoiling angle: the torque, after a nearly linear increase, becomes almost supercoiling-independent while the writhe-to-twist ratio, initially confined to the 20% level develops a fast linear increase. This behaviour is reminiscent of the buckling instability of a twisted rubber tube associated with the creation of plectonemes, able to absorb supercoiling at constant torque. We have shown that the configurations excited in the RLC model above the critical value χ_{c} share a simple global symmetry property with a set of undeformed plectonemes arbitrarily oriented with respect to the force direction z-axis: the angular distribution of the tangent vector $\hat{\mathbf{t}}$ has a forward backward symmetry with respect to the z-axis. The existence of this rather sharp cross over has been confirmed by an analysis of the extension fluctuations *versus* supercoiling: the predicted fluctuations jump near χ_{c} is clearly seen on the preliminary experimental data.

The overall good agreement of our predictions with the analyzed experimental data seems to indicate that the self-avoiding effects, not included in our RLC model, play a limited role in the low supercoiling regime $|\sigma| \leq 0.02$. This was suggested by the Monte Carlo simulations of Marko and Vologodskii [30] who use two infinite impenetrable walls to adapt the closed chain formalism to the supercoiled open chains. A further test follows from computing $\lim_{F=0}\langle \chi_W\rangle/\chi$ for σ values taken in the range $0 \leq -\sigma \leq 0.04$. This ratio compares well to the closed DNA chain writhe average $\langle Wr/\Delta Lk\rangle$ obtained by Monte Carlo simulations [29]. The two results diverge by less than 10% when $|\sigma| \leq 0.04$ and both agree with the experimental data within errors [26,27]. It should be said that the two calculations use different formulas for the writhe: an open chain local version in the present paper, the non-local loop geometrical formula [23] in reference [29].

In view of the wealth of experimental information, there are strong motivations to extend the validity of the present RLC model to a larger domain of the (F,σ)-plane. Further work has to be pursued in several directions. Non-local constraints in the chain tangent vector $\hat{\mathbf{t}}$ space have to be implemented. There are first the empirical geometrical constraints associated with the DNA anchoring glass plate and the finite radius of the tracking bead. The self-avoiding effects induced by the Coulomb repulsion within the DNA chain have to be studied for the range of ionic strength accessible to experiments. The only practical approach to these problems seems, for the moment, the Monte Carlo simulations technique.

Another interesting perspective is to incorporate in the present model the double-helix structure of the DNA, in order to describe the DNA denaturation transition induced by negative supercoiling above $F = 0.5\,\mathrm{pN}$. Some first steps in this direction have already been taken in [13, 14]. Recently a model coupling the hydrogen-bond opening with the untwisting of the double helix has been proposed [15]. It allows a unified description of DNA denaturation driven by thermal fluctuations or induced by the double-helix untwisting, in the case of a straight line molecular chain. It will be of interest to combine this model with the elastic RLC model in order to study the onset of the denaturation transition at moderate stretching forces, say below 1 pN, where bending fluctuations can no longer be neglected.

It is a great pleasure to thank all members of the experimental group at ENS, J.-F. Allemand, D. Bensimon, V. Croquette and T.R. Strick, for many valuable discussion, and for providing us with some of their unpublished data. We have benefited from discussions with J.-P. Bouchaud, A. Comtet and C. Monthus

on the winding of random walks. We are very grateful to D. Bensimon and M.A. Bouchiat for their careful reading of this long manuscript. The work of MM was supported in part by the National Science Foundation under grant No. PHY94-07194.

Appendix A. Rotation matrix algebra

Let us denote by $R(\hat{\mathbf{n}},\gamma)$ the rotation of angle γ about the unitary vector $\hat{\mathbf{n}}$. With this notation, the rotation $\mathcal{R}(s)$, which specifies an arbitrary DNA chain configuration in terms of the three Euler angles, is given by

$$\mathcal{R}(s) = R(\hat{\mathbf{z}},\phi(s))R(\hat{\mathbf{y}},\theta(s))R(\hat{\mathbf{z}},\psi(s)). \tag{A.1}$$

Another very useful way of writing $\mathcal{R}(s)$ follows from the rotation group relation:

$$\hat{R} = R_1^{-1}R(\hat{\mathbf{n}},\gamma)R_1 = R\big(R_1^{-1}\hat{\mathbf{n}},\gamma\big). \tag{A.2}$$

The proof of (A.2) follows from the basic properties of a rotation matrix: first, the rotation axis is the rotation matrix eigenvector with unit eigenvalue; we verify that it is indeed the case for $R_1^{-1}\hat{\mathbf{n}}$: $\hat{R}R_1^{-1}\hat{\mathbf{n}} = R_1^{-1}R(\hat{\mathbf{n}},\gamma)\hat{\mathbf{n}} = R_1^{-1}\hat{\mathbf{n}}$; second, the rotations $\hat{R}$ and $R(\hat{\mathbf{n}},\gamma)$ have, by construction, the same eigenvalues: 1, $\exp(i\gamma)$, $\exp(-i\gamma)$ and hence the same rotation angle γ. The new form of $\mathcal{R}(s)$ is then obtained from the simple manipulations

$$\begin{aligned}\mathcal{R}(s) &= R(\hat{\mathbf{z}},\phi)R(\hat{\mathbf{y}},\theta)R(\hat{\mathbf{z}},\psi)\\ &= R(\hat{\mathbf{z}},\phi+\psi)R^{-1}(\hat{\mathbf{z}},\psi)R(\hat{\mathbf{y}},\theta)R(\hat{\mathbf{z}},\psi)\\ &= R(\hat{\mathbf{z}},\phi+\psi)R(R(\hat{\mathbf{z}},-\psi)\hat{\mathbf{y}},\theta).\end{aligned} \tag{A.3}$$

We are going now to discuss the two angular velocity vectors and $\boldsymbol{\Omega}(s)$ and $\boldsymbol{\Upsilon}(s)$ defined by relations valid for arbitrary vectors $\mathbf{X}$ and $\mathbf{Y}$:

$$\dot{\mathcal{R}}(s)\mathcal{R}^{-1}(s)\mathbf{X} = \boldsymbol{\Omega}(s)\wedge\mathbf{X}, \tag{A.4}$$

$$\mathcal{R}^{-1}(s)\dot{\mathcal{R}}(s)\mathbf{Y} = \boldsymbol{\Upsilon}(s)\wedge\mathbf{Y}. \tag{A.5}$$

Applying to equation (A.5) the simple identity $\mathcal{R}(\mathbf{a}\wedge\mathbf{b}) = (\mathcal{R}\mathbf{a})\wedge(\mathcal{R}\mathbf{b})$ and taking $\mathbf{Y} = \mathcal{R}^{-1}(s)\mathbf{X}$, one gets immediately the relation $\boldsymbol{\Omega}(s) = \mathcal{R}(s)\boldsymbol{\Upsilon}(s)$. It facilitates the evaluation of the components of $\boldsymbol{\Omega}(s)$ upon the moving trihedron $\{\hat{\mathbf{e}}_i(s)\}$ since we can write

$$\Omega_i = \boldsymbol{\Omega}(s)\cdot\hat{\mathbf{e}}_i(s) = \boldsymbol{\Upsilon}(s)\cdot\hat{\mathbf{e}}_i^0(s). \tag{A.6}$$

To simplify the writing in the explicit computation of $\boldsymbol{\Upsilon}(s)$, we introduce the notations $R_1 = R(\hat{\mathbf{z}},\phi(s))$, $R_2 = R(\hat{\mathbf{y}},\theta(s))$, $R_3 = R(\hat{\mathbf{z}},\psi(s))$. With some elementary matrix algebra we get

$$\begin{aligned}\mathcal{R}^{-1}(s)\dot{\mathcal{R}}(s) = (R_2R_3)^{-1}&R_1^{-1}\dot{R}_1R_2R_3\\ &+ R_3^{-1}R_2^{-1}\dot{R}_2R_3 + R_3\dot{R}_3.\end{aligned}$$

As an intermediary step, we compute

$$\begin{aligned}R_a^{-1}R^{-1}(\hat{\mathbf{n}},\gamma(s))\dot{R}(\hat{\mathbf{n}},\gamma(s))R_a\mathbf{X} &=\\ R_a^{-1}(\dot{\gamma}(s)\hat{\mathbf{n}}\wedge R_a\mathbf{X}) &= \dot{\gamma}R_a^{-1}\hat{\mathbf{n}}\wedge\mathbf{X}.\end{aligned}$$

This result is nothing but relation (A.2) applied to an infinitesimal rotation. Using the above results, we arrive finally at the following expression for $\boldsymbol{\Upsilon}(s)$:

$$\boldsymbol{\Upsilon}(s) = \dot{\phi}R(\hat{\mathbf{z}},-\psi)R(\hat{\mathbf{y}},-\theta)\hat{\mathbf{z}} + \dot{\theta}R(\hat{\mathbf{z}},-\psi)\hat{\mathbf{y}} + \dot{\psi}\hat{\mathbf{z}}. \tag{A.7}$$

It is now convenient to decompose $\boldsymbol{\Upsilon}(s)$ in a longitudinal $\boldsymbol{\Upsilon}_\parallel(s)$ and a transverse part $\boldsymbol{\Upsilon}_\perp(s)$

$$\boldsymbol{\Upsilon}_\parallel = (\cos\theta\dot{\phi} + \dot{\psi})\hat{\mathbf{z}}, \tag{A.8}$$

$$\boldsymbol{\Upsilon}_\perp = R(\hat{\mathbf{z}},-\psi)(-\dot{\phi}\sin\theta\hat{\mathbf{x}} + \dot{\theta}\hat{\mathbf{y}}). \tag{A.9}$$

We get immediately the quantities appearing in the RLC elastic energy

$$\Omega_3 = \cos\theta\dot{\phi} + \dot{\psi}, \tag{A.10}$$

$$\Omega_\perp{}^2 = \boldsymbol{\Upsilon}_\perp^2 = \Omega_1^2 + \Omega_2^2 = \dot{\phi}^2\sin^2\theta + \dot{\theta}^2. \tag{A.11}$$

Our next step is to compute the cylindrical symmetry breaking term $\Delta\Omega(s) = \Omega_1^2 - \Omega_2^2$. Introducing the angle $\zeta(s) = \arctan(\dot{\theta}/(\sin\theta\dot{\phi}))$, we can write: $\boldsymbol{\Upsilon}_\perp = -\Omega_\perp R(\hat{\mathbf{z}},-\psi-\zeta)\hat{\mathbf{x}}$. A physical interpretation of $\zeta(s)$ is obtained by computing the s derivative of the tangent unit vector $\hat{\mathbf{t}}(s)$:

$$\begin{aligned}\frac{\mathrm{d}\hat{\mathbf{t}}(s)}{\mathrm{d}s} &= \boldsymbol{\Omega}\wedge\hat{\mathbf{t}} = \mathcal{R}(s)(\boldsymbol{\Upsilon}_\perp\wedge\hat{\mathbf{z}})\\ &= -\Omega_\perp\mathcal{R}(s)R(\hat{\mathbf{z}},-\psi-\zeta)(\hat{\mathbf{x}}\wedge\hat{\mathbf{z}})\\ &= \Omega_\perp R(\hat{\mathbf{z}},\phi)R(\hat{\mathbf{y}},\theta)R(\hat{\mathbf{z}},-\zeta)\hat{\mathbf{y}}.\end{aligned}$$

We see that $-\zeta(s)$ plays the role of the Euler angle $\psi(s)$ *vis-à-vis* the Seret-Frenet trihedron so that $\zeta(s)$ is clearly connected with the writhe. It is now a simple matter to get the component Ω_1 by writing the series of equalities

$$\begin{aligned}\Omega_1 = \boldsymbol{\Upsilon}(s)\cdot\hat{\mathbf{e}}_1^0(s) =&\\ &-\Omega_\perp(R(\hat{\mathbf{z}},-\psi-\zeta)\hat{\mathbf{x}})\cdot(R(\hat{\mathbf{z}},\omega_0 s)\hat{\mathbf{x}}) =\\ &-\Omega_\perp\hat{\mathbf{x}}\cdot(R(\hat{\mathbf{z}},\psi+\zeta+\omega_0 s)\hat{\mathbf{x}}) =\\ &-\Omega_\perp\cos(\psi+\zeta+\omega_0 s).\end{aligned}$$

In a similar way we obtain $\Omega_1 = -\Omega_\perp\sin(\psi+\zeta+\omega_0 s)$ and we arrive finally at the following expression for $\Delta\Omega(s)$:

$$\Delta\Omega(s) = \Omega_1^2 - \Omega_2^2 = \Omega_\perp{}^2\cos 2(\psi+\zeta+\omega_0 s). \tag{A.12}$$

Introducing the length resolution function $P(s) = (1/\sqrt{2\pi}\ell)\exp(-\frac{1}{2}s^2/\ell^2)$ (note the change of notation: ℓ stands for Δl used in the main body of the paper), we proceed with the computation of the average $\overline{\Delta\Omega(s)}$:

$$\begin{aligned}\overline{\Delta\Omega(s)} = &\int \mathrm{d}s_1 P(s_1-s)\Delta\Omega(s_1) =\\ &\frac{1}{\sqrt{2\pi}}\int \mathrm{d}u\exp\left(-\frac{1}{2}u^2\right)\Delta\Omega(s+u\ell).\end{aligned}$$

Let us first neglect the variation of $\Omega_\perp$ within the interval $(s-\ell, s+\ell)$ and perform a first-order expansion in ℓ of the phase $\psi(s+u\ell)+\zeta(s+u\ell)$; this is justified since

its variation is expected to be of the order of $(\ell/A) \approx 0.2$ (we have proved explicitly the thermal average inequality $\langle\dot{\psi}\rangle/\eta < 1/A$). In this way $\overline{\Delta\Omega(s)}$ is transformed into a Gauss integral

$$\overline{\Delta\Omega(s)} = \Delta\Omega(s)\frac{1}{\sqrt{2\pi}} \times \int \mathrm{d}u \exp\Big(-\frac{1}{2}u^2\Big)\cos(2u\ell(\dot{\psi}+\dot{\zeta}+\omega_0)) = \Delta\Omega(s)\exp\big(-2\ell^2(\dot{\psi}+\dot{\zeta}+\omega_0)^2\big). \quad \text{(A.13)}$$

Using the estimates $|\dot{\psi}|/\omega_0| \sim |\dot{\zeta}|/\omega_0 \sim |\chi|/(L\omega_0) = |\sigma|$ and the fact that in the present paper our analysis is restricted to values of $|\sigma| < 4\cdot 10^{-2}$, we can write, introducing the pitch $p = 2\pi/\omega_0$,

$$\overline{\Delta\Omega(s)} \approx \Delta\Omega(s)\exp\Big(-\frac{1}{2}\Big(\frac{4\pi\ell}{p}\Big)^2\Big). \quad \text{(A.14)}$$

Taking $p = 3.4\,\mathrm{nm}$, $\ell = 10\,\mathrm{nm}$, we find $(4\pi\ell/p) \approx 37$; it means that $\overline{\Delta\Omega(s)}/\Delta\Omega(s)$ is zero for all practical purposes. Using instead $\ell = b = 7\,\mathrm{nm}$ would not make any difference. Let us say few words about the term $\delta\overline{\Delta\Omega(s)}$ involving the variation of ${\Omega_\perp}^2$. A computation similar to the previous one gives the following result:

$$\delta\overline{\Delta\Omega(s)} = \frac{\partial {\Omega_\perp}^2}{\partial s}\ell\frac{4\pi\ell}{p}\exp\Big(-\frac{1}{2}\Big(\frac{4\pi\ell}{p}\Big)^2\Big) \times \sin 2(\psi+\zeta+\omega_0 s).$$

The rate of variation of ${\Omega_\perp}^2$, which is the inverse of the curvature radius square, is expected to be of the order $1/A$ so that $(1/{\Omega_\perp}^2)(\partial{\Omega_\perp}^2/\partial s)\ell \sim \ell/A = 0.2$. It follows that $\delta\overline{\Delta\Omega(s)}$ is still exceedingly small compared to $\Delta\Omega(s)$. Furthermore it is easily shown that the thermal average derivative $(\partial\langle{\Omega_\perp}^2\rangle/\partial s)$ vanishes for $s \gg A$.

Appendix B. The symmetric top and the RLC model

In this appendix we shall use for convenience a unit system where $\hbar = c = k_\mathrm{B}T = 1$ and write $\Im s = t$. The elastic energy E_RLC (Eq. (2) and Eq. (3)) is transformed by an analytic continuation towards the imaginary s-axis into $-i$ times the action integral:

$$\mathcal{A}(t_0,t_1) = \int_{t_0}^{t_1}\mathrm{d}t\bigg(\frac{1}{2}\sum_{j=1}^{3}C_j\Omega_j^2 + f\cos\theta(t)\bigg),$$

where $C_1 = C_2 = A$, $C_3 = C$ and $f = F/(k_\mathrm{B}T)$. The time derivative accounts for the relative change of sign between $C_i\Omega_i^2$ and the potential energy $-f\cos\theta(t)$. The analytically continued partition function of the RLC model is then identified with the Feynmann path integral amplitude

$$\big\langle\theta_1,\phi_1,\psi_1,t_1|\theta_0,\phi_0,\psi_0,t_0\big\rangle = \int\mathcal{D}(\theta,\phi,\psi)\exp\bigg(i\int_{t_0}^{t_1}\mathrm{d}t\mathcal{L}_\mathrm{top}(t)\bigg).$$

The Lagrangian $\mathcal{L}_\mathrm{top}(t) = \frac{1}{2}\sum_1^3 C_i\Omega_i^2 + f\cos\theta(t)$ describes the motion of a spherical top with inertia moments $I_i = C_i$, under the action of a static electric field E_0. (The molecular electric moment is given by f/E_0.) In order to compute explicitly the Hamiltonian $\mathcal{H}_\mathrm{top}$, let us write $\mathcal{L}_\mathrm{top}(t)$ in terms of the Euler angles and their derivatives:

$$\mathcal{L}_\mathrm{top} = \frac{A}{2}\big(\dot{\phi}^2\sin^2\theta+\dot{\theta}^2\big) + \frac{C}{2}\big(\dot{\psi}+\dot{\phi}\cos\theta\big)^2 + f\cos\theta. \quad \text{(B.1)}$$

One gets immediately the conjugate momentums relative to three Euler angles: $p_\phi = A\sin^2\theta\dot{\phi}+\cos\theta p_\psi$, $p_\psi = C(\dot{\psi}+\dot{\phi}\cos\theta)$ and $p_\theta = A\dot{\theta}$. The symmetric top Hamiltonian is then readily obtained

$$\mathcal{H}_\mathrm{top} = \frac{A}{2}\big(\dot{\phi}^2\sin^2\theta+\dot{\theta}^2\big) + \frac{C}{2}(\dot{\psi}+\dot{\phi}\cos\theta)^2 - f\cos\theta = \frac{(p_\phi-\cos\theta p_\psi)^2}{2A\sin^2\theta} + \frac{{p_\theta}^2}{2A} + \frac{{p_\psi}^2}{2C} - f\cos\theta. \quad \text{(B.2)}$$

To get the Hamiltonian operator $\hat{\mathcal{H}}_\mathrm{top}$, we apply the standard quantization rules

$$p_\phi \to \hat{p}_\phi = \frac{\partial}{i\partial\phi}, \qquad p_\psi \to \hat{p}_\psi = \frac{\partial}{i\partial\psi},$$
$$p_\theta^2 \to \hat{p}_\theta^2 = -\frac{1}{\sin\theta}\frac{\partial}{\partial\theta}\sin\theta\frac{\partial}{\partial\theta}.$$

To get the partition function $Z(\theta_1,\phi_1,\psi_1,s_1|\theta_0,\phi_0,\psi_0,s_0)$ we expand the final and initial states upon eigenfuctions of the operators $\hat{p}_\phi$ and $\hat{p}_\psi$: $\exp(im\phi+ik\psi)$, where k and m are arbitrary real numbers, in contrast with the real symmetric top case, where they are integers. This difference, which follows from a detailed analysis of the physics involved (see section 2.2 for details), is responsible for the singular features of the continuous RLC model. The partition function with the notations used in the paper to label the initial and final states reads as follows:

$$Z(\theta(L),\phi(L),\psi(L),L|\theta(0),0) = \int\mathrm{d}m\,\mathrm{d}k\exp(im\phi(L)+ik\psi(L)) \times\langle\theta(L)|\exp(-L\hat{\mathcal{K}}(k,m))|\theta(0)\rangle, \quad \text{(B.3)}$$

where the Hamiltonian $\hat{\mathcal{K}}(k,m)$ is given by

$$\hat{\mathcal{K}}(k,m) = -\frac{1}{2A\sin\theta}\frac{\partial}{\partial\theta}\sin\theta\frac{\partial}{\partial\theta} + \frac{(m-\cos\theta k)^2}{2A\sin^2\theta} + \frac{k^2}{2C} - f\cos\theta.$$

The experimental supercoiling constraint is implemented by averaging upon $\phi(L)$ and $\psi(L)$ the above partition function multiplied by the Dirac function $\delta(\phi(L)+\psi(L)-\chi)$. A straightforward computation gives

$$Z(\chi) = \int\mathrm{d}k\exp(ik\chi)\big\langle\theta(L)\big|\exp\big(-L\hat{\mathcal{K}}(k,k)\big)\big|\theta(0)\big\rangle.$$

The Hamiltonian operator $\hat{H}_{\rm RLC}(k)$ given by equation (16) is recovered by writing

$$\hat{H}_{\rm RLC}(k) = \frac{1}{A}\left(\hat{\mathcal{K}}(k,k) - \frac{A}{2C}k^2\right)$$
$$= -\frac{1}{2\sin\theta}\,\frac{\partial}{\partial\theta}\sin\theta\frac{\partial}{\partial\theta} - \alpha\cos\theta + \frac{k^2}{2}\,\frac{1-\cos\theta}{1+\cos\theta}\,. \quad \text{(B.4)}$$

The merit of this direct derivation is to show clearly that k is the unquantized angular momentum of the Euclidian symmetric top problem associated with the RLC model. It is the breaking of the quantum mechanics usual quantization rule which is at the origin of the RLC model pathology.

References

1. S.B. Smith, L. Finzi, C. Bustamante, Science **258**, 1122 (1992).
2. T.T. Perkins, S.R. Quake, D.E. Smith, S. Chu, Science **264**, 8222 (1994).
3. T.R. Strick, J.-F. Allemand, D. Bensimon, A. Bensimon, V. Croquette, Science **271**, 1835 (1996).
4. C. Bustamante, J.F. Marko, E.D. Siggia, S. Smith, Science **265**, 1599 (1994); A. Vologodskii, Macromolecules **27**, 5623 (1994).
5. M. Fixman, J. Kovac, J. Chem. Phys. **58**, 1564 (1973).
6. P. Cluzel, A. Lebrun, C. Heller, R. Lavery, J.L. Viovy, D. Chatenay, F. Caron, Science **271**, 792 (1996); S.B. Smith, Y. Cui, C. Bustamante, Science **271**, 795 (1996).
7. T.R. Strick, J.-F. Allemand, D. Bensimon, V. Croquette, Biophys. J. **74**, 2016 (1998).
8. T.R.Strick, V. Croquette, D. Bensimon, Proc. Natl. Acad. Sci. USA **95**, 10579 (1998).
9. T.R.Strick, D. Bensimon, V. Croquette, Genetica **106**, 57 (1999).
10. C. Bouchiat, M.D. Wang, S.M. Block, J.-F. Allemand, V. Croquette, Biophys. J. **76**, 409 (1999).
11. J.-F. Allemand, D. Bensimon, R. Lavery, V. Croquette, Proc. Natl. Acad. Sci (USA) **95**, 14152 (1998).
12. C. Bouchiat, M. Mézard, Phys. Rev. Lett. **80**, 1556 (1998).
13. T.B. Liverpool, R. Golestanian, K. Kremer, Phys. Rev. Lett. **80**, 405 (1998).
14. Zhou Haijun, Z.C. Ou-Yang, cond-mat/9901321.
15. S. Cocco, R. Monasson, Phys. Rev. Lett. **83**, 5178 (1999).
16. B. Fain, J. Rudnick, cond-mat/9903364.
17. J.F. Marko, E.D. Siggia, Science **265**, 506 (1994); Phys. Rev. E **52**, 2912 (1995).
18. D. Bensimon, D. Dohmi, M. Mézard, Europhys. Lett. **42**, 97 (1998).
19. J.F. Marko, Europhys. Lett. **38**, 183 (1997); Phys. Rev. E **57**, 2134 (1998).
20. R.D. Kamien, T.C. Lubensky, P. Nelson, C.S. O'Hern, Europhys. Lett. **38**, 237 (1997).
21. J.D. Moroz, P. Nelson, Proc. Natl. Acad. Sci. USA **94**, 14418 (1997).
22. J.D. Moroz, P. Nelson, Macromolecules **3**, 6333 (1998).
23. J.H. White, Am. J. Math. **91**, 693 (1969); F.B. Fuller, Proc. Nat. Acad. Sci. USA **68**, 815 (1971).
24. F.B. Fuller, Proc. Nat. Acad. Sci. USA **75**, 3557 (1978).
25. B. Fain, J. Rudnick, S. Östlund, Phys. Rev. E **55**, 7364 (1997).
26. T.C. Boles, J.H. White, N.R. Cozzarelli, J. Mol. Biol. **213**, 931 (1990).
27. M. Adrian, B. ten Heggeler-Bordier, W. Whali, A.Z. Stasiak, A. Stasiak, J. Dubochet., Eur. Mol. Biol. Org. J. **13**, 451
28. See the discussion in A. Comtet, J. Desbois, C. Monthus, J. Stat. Phys. **73**, 433 (1993), and references therein, particularly: F. Spizer, Trans. Am. Math. Soc. **87**, 187 (1958); C. Belisle, Ann. Prob. **17**, 1377 (1989).
29. See A.V. Vologodskii, S.D. Levene, K.V. Klenin, M. Frank-Kamenetskii, N.R. Cozzarelli, J. Mol. Biol. **227**, 1224 (1992) and references therein.
30. J.F. Marko, A.V. Vologodskii, Biophys. J. **73**, 123 (1997).